Journal of Asian Earth Sciences 62 (2013) 18–36

Contents lists available at SciVerse ScienceDirect

Journal of Asian Earth Sciences

journal homepage: www.elsevier.com/locate/jseaes

Zircon ages and Hf isotopic constraints on sources of clastic metasediments of the Slyudyansky high-grade complex, southeastern Siberia: Implication for continental growth and evolution of the Central Asian Orogenic Belt

Victor Kovach [a,*], Ekaterina Salnikova [a], Kuo-Lung Wang [b], Bor-Ming Jahn [b,c], Han-Yi Chiu [c], Leonid Reznitskiy [d], Alexander Kotov [a], Yoshiyuki Iizuka [b], Sun-Lin Chung [c]

[a] Institute of Precambrian Geology and Geochronology, Russian Academy of Sciences, St. Petersburg, Russia
[b] Institute of Earth Sciences, Academia Sinica, Taipei, Taiwan
[c] Department of Geosciences, National Taiwan University, Taipei, Taiwan
[d] Institute of the Earth Crust, Siberian Branch, Russian Academy of Sciences, Irkutsk, Russia

ARTICLE INFO

Article history:
Available online 13 September 2011

Keywords:
Central Asian Orogenic Belt
Slyudyansky Complex
Zircon ages
Nd–Hf isotopes
Continental growth

ABSTRACT

We present results of combined in situ U–Pb dating of detrital zircons and zircon Hf and whole-rock Nd isotopic compositions for high-grade clastic metasedimentary rocks of the Slyudyansky Complex in eastern Siberia. This complex is located southwest of Lake Baikal and is part of an early Paleozoic metamorphic terrane in the eastern part of the Central Asian Orogenic Belt (CAOB). Our new zircon ages and Hf isotopic data as well as whole-rock Nd isotopic compositions provide important constraints on the time of deposition and provenance of early Paleozoic high-grade metasedimentary rocks as well as models of crustal growth in Central Asia. Ages of 0.49–0.90 Ga for detrital zircons from early Paleozoic high-grade clastic sediments indicate that deposition occurred in the late Neoproterozoic and early Paleozoic, between ca. 0.62–0.69 and 0.49–0.54 Ga. Hf isotopic data of 0.82–0.69 Ga zircons suggest Archean and Paleoproterozoic (ca. 2.7–2.8 and 2.2–2.3 Ga; Hfc = 2.5–3.9 Ga) sources that were affected by juvenile 0.69–0.82 Ga Neoproterozoic magmatism. An additional protolith was also identified. Its zircons yielded ages of 2.6–2.7 Ga, and showed high positive $\varepsilon_{Hf}(t)$ values of +4.1 to +8.0, and Hf model ages $t_{Hf(DM)} = t_{Hfc}$ = 2.6–2.8 Ga, which is nearly identical to the crystallization ages. These isotopic characteristics suggest that the protolith was quite juvenile. The whole-rock Nd isotopic data indicate that at least part of the Slyudyansky Complex metasediments was derived from "non-Siberian" provenances. The crustal development in the eastern CAOB was characterized by reworking of the early Precambrian continental crust in the early Neoproterozoic and the late Neoproterozoic–early Paleozoic juvenile crust formation.

1. Introduction

The Central Asian Orogenic Belt (CAOB) (Jahn et al., 2000) also known as Central Asian fold belt (Zonenshain et al., 1990) or Altaid tectonic collage (Sengör et al., 1993) is located between the Siberian craton in the north and the Sino-Korean (North China) and Tarim cratons in the south and encompasses an immense area from the Urals, through Kazakhstan, NW China, Mongolia, southern Siberia, NE China to the Okhotsk Sea in the Russian Far East (Fig. 1). The geological structure of the CAOB (Fig. 2) is defined by a combination of microcontinents, Paleozoic high-grade metamorphic complexes and mobile belts of different age from the Neoproterozoic to the Mesozoic (Mossakovsky et al., 1993; Sengör et al., 1993; Dergunov et al., 2001; Kovalenko et al., 2004). These mobile belts comprised by oceanic, island arc, back-arc/fore-arc, active continental margin and other complexes intruded by voluminous granitods.

The microcontinents of the CAOB are composed of high-grade metamorphic complexes and a late Neoproterozoic to Cambrian sedimentary cover. In the past, they have often been considered as early Precambrian basement of Neoproterozoic and Phanerozoic mobile belts (Early Precambrian..., 1993; Tectonic map..., 1979; Atlas of geological maps..., 2007; Il'in, 1971, 1982). However, geological and geochronological investigations have since demonstrated that early Precambrian high-grade rocks are rare within the CAOB and do not make up more than 1–2% of total area. Most high-grade complexes have experienced amphibolite- to granulite-facies metamorphism in Neoproterozoic or Paleozoic times (e.g., Kotov et al., 1997; Kozakov et al., 1999, 2001, 2004, 2007a,b, 2008; Salnikova

* Corresponding author.
E-mail address: v.p.kovach@gmail.com (V. Kovach).

1367-9120/$ - see front matter © 2011 Elsevier Ltd. All rights reserved.
doi:10.1016/j.jseaes.2011.08.008

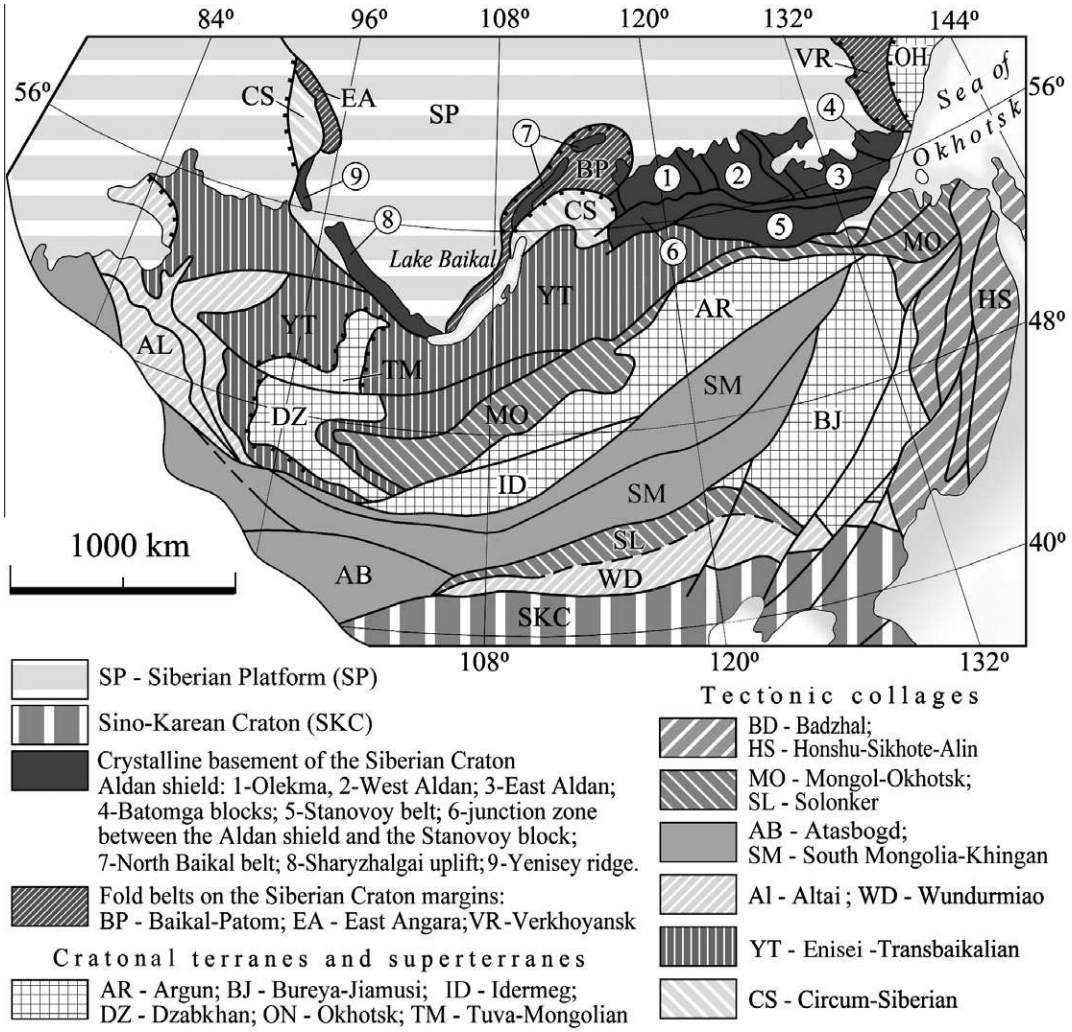

Fig. 1. Scketch map showing position and tectonic units of the part of the Central Asian Orogenic Belt and the southern Siberian craton. Modified from Nokleberg et al. (2004).

et al., 1998, 2001; Donskaya et al., 2000; Yarmolyuk et al., 2005a,b; Gladkochub et al., 2010; Rytsk et al., 2009; Demoux et al., 2009a,b,c). On this basis the Neoproterozoic to Paleozoic high-grade complexes were separated from true Precambrian microcontinents as metamorphic terranes (belts) of uncertain tectonic affinity (Badarch et al., 2002; Parfenov et al., 2004)

There has been much controversy concerning the origin and evolution of the CAOB microcontinents and high-grade metamorphic belts. Some authors suggested that at least some microcontinents were rifted off Gondwana (Mossakovsky et al., 1993; Didenko et al., 1994; Kheraskova et al., 2003, 2010; Dobretsov and Buslov, 2007), whereas others assumed that they were separated from the Siberian craton (Berzin et al., 1994; Kuzmichev, 2004; Turkina et al., 2007). Another viewpoint suggested that the basement of, for instance, the Tuva–Mongolian microcontinent is composed of metamorphosed Neoproterozoic volcanic arc and sedimentary assemblages (Kozakov et al., 2005) that may have formed in the Pantalassa Ocean around the margins and on the shelf of the Rodinia supercontinent (Yarmolyuk and Kovalenko, 2001; Yarmolyuk et al., 2005b, 2006). The latest Neoproterozoic and early Paleozoic high-grade metamorphic events were thought to be related to accretion and collision processes during the formation of the early Paleozoic superterrane of Central Asia (Kozakov et al., 2005, 2008; Kovalenko et al., 2004; Yarmolyuk et al., 2006). Because the provenance of sedimentary rocks may provide paleogeographic constraints, the questions of depositional age and provenance of metasedimentary rocks in the high-grade terranes are critical for understanding crustal growth and evolution of the CAOB.

Zircon dating helps to determine the age of sedimentary source material and therefore constrains the older limit of sediment deposition and possible provenance. Due to the relative resistance of Hf isotopes in zircon to alteration (Patchett et al., 1981; Fujimaki, 1986) and the close correspondence of magmatic zircon Hf isotopic composition to whole-rock Nd isotopic composition at the time of zircon growth, the combination of zircon ages and Hf isotopes becomes a powerful tool to study the formation age and protolith nature of metasedimentary rocks (e.g., Patchett et al., 1981; Vervoort and Patchett, 1996; Blichert-Toft and Albarède ,1997; Scherer et al., 1997, 2000; Amelin et al., 1999). We present first results of a combined in situ analysis of detrital zircon ages as well as zircon Hf and whole-rock Nd isotopic compositions for high-grade metasedimentary rocks of the Slyudyansky Complex of the southeastern Siberia.

2. Geological setting and previous geochronological studies

The Slyudyansky Complex is situated southwest of Lake Baikal, in the eastern part of the CAOB, and is separated by the Main Sayan Fault from the Sharyzhalgay Complex of the Siberian craton

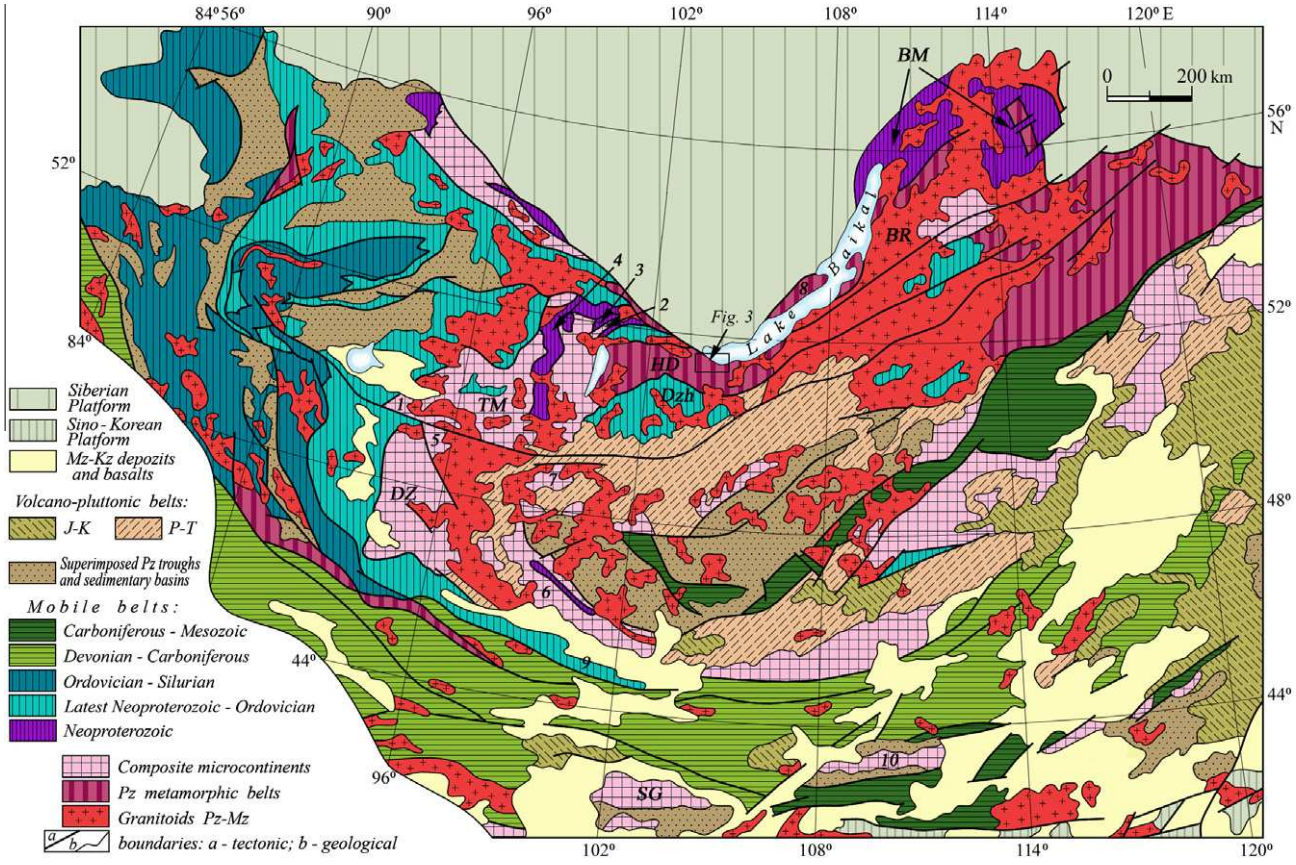

Fig. 2. Simplified geological map of the eastern part of the Central Asian Orogenic Belt. Modified from the terrane map of Parfenov et al. (2004). Units discussed in the text: TM – Tuva–Mongolian, DZ – Dzabkhan, SG – microcontinents; BM – Baikal-Muya, Dzh – Dhida, HD – Hamar-Davaa belts; BR – Barguzin superterrane; 1 – Western Sangilen, 2 – Gargan blocks of the Tuva–Mongolian microcontinent; 3 – Dunzhugur, 4 – Shishkhid, Oka and Sarkhoy belts; 5 – Songino, 6 – Baidrag, 7 – Tarbagatai blocks of the Dzabkhan microcontinent; 9 – approximate location of the Baga Bogd block; 10 – Totoshan-Ulanul block of the South Gobi microcontinent. The approximate location of Fig. 3 is indicated.

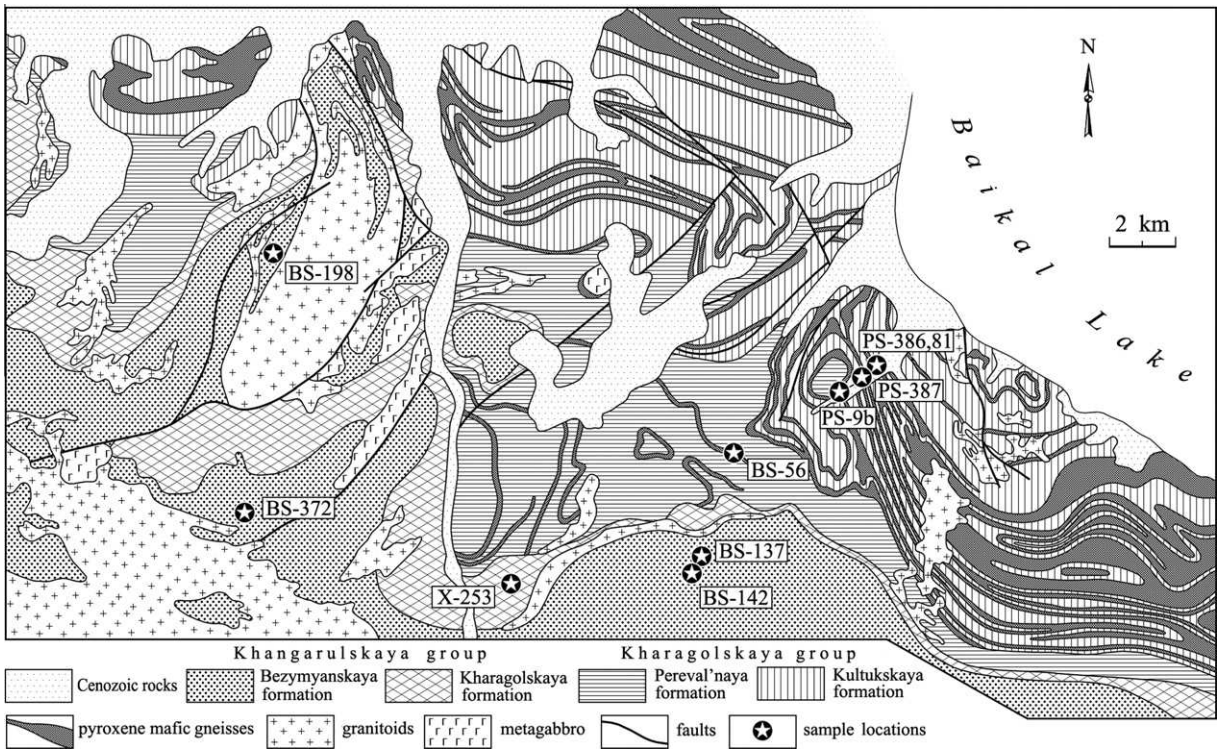

Fig. 3. Simplified geological map of the Slyudyansky high-grade complex. Compiled from Vasil'ev et al. (1981).

(Fig. 2). The complex is composed of granulite-facies supracrustal rocks of the Slyudyanskaya and Khangarulskaya "series" and was traditionally regarded as Eo- or Paleoarchean in age (Tectonic map. . ., 1979; Il'in, 1982; Mossakovsky et al., 1993). Together with high-grade metamorphic rocks of the Western Sangilen and Khamar-Daban Range, it was also considered as an elevated part of the Tuva–Mongolian microcontinent unconformably overlain by a late Neoproterozoic (Vendian) to Cambrian carbonate cover sequence (Il'in, 1982). Subsequently, the Slyudyansky Complex, together with the Hamardaban Complex, was classified as the Hamar-Davaa metamorphic terrane of uncertain tectonic affinity (Belichenko et al., 1994; Badarch et al., 2002; Parfenov et al., 2004). The Hamar-Davaa terrane extends northeast from Lake Khubsugul (northern Mongolia) in the south through the Khamar-Daban Range and farther along Lake Baikal (Fig. 2). It consists of metamorphic rocks of the Slyudyanskaya, Khangarulskaya and Khamardabanskaya "series" of unknown ages, assumed to be from the Archean to the Paleozoic (Vasil'ev and Reznitskiy, 1993; Belichenko and Boos, 1988). Because of rocks of the Hamar-Davaa terrane are highly deformed and metamorphosed, their subdivision on "series" is only tectono-stratigraphic. Recent zircon dating (Barash et al., 2006) showed that high-temperature metamorphism in the Hamardaban Complex occurred at 495 ± 2 Ma, whereas granulite-facies metamorphism and emplacement of syntectonic granitoids into the Slyudyansky Complex was dated at 488–478 Ma (Salnikova et al., 1998). These data suggest that granulite-facies metamorphism in the Slyudyansky Complex postdated the high-temperature metamorphism in the Hamardaban Complex. However, it is uncertain whether or not metamorphic zonality in the Hamardaban Complex and granulite-facies metamorphism in the Slyudyansky Complex mark different tectonic events or reflect a long-lasting, single event.

Detailed structural and metamorphic work on the Slyudyansky Complex (Fig. 3) was undertaken by several workers such as Shafeev (1970), Vasil'ev et al. (1981), and Vasil'ev and Reznitskiy (1993). The complex consists of marble, calc-silicate rocks, hornblende–pyroxene schist and various paragneisses (grt-bt-sill, grt-bt, bt-grt-hy-crd, grt-bt-sil-crd, grt-sil-cord-bt, bt-grt-crd, bt-grt-hy and bt-2px gneisses) of the Slyudanskaya "series" and of calcareous diopside schist, gneiss, metapelite and marble of the Khangarulskaya "series" (Vasil'ev and Reznitskiy, 1993). The Slyudanskaya "series" is subdivided into two sub-units, namely the lower Kultukskaya and upper Pereval'naya "suites". The Kultukskaya "suite" contains a roughly equal amount of carbonate and aluminosilicate rocks, whereas carbonate rocks dominate in the Pereval'naya "suite". All rocks of the Slyudyansky Complex have undergone granulite-facies metamorphism and were subjected to four phases of ductile deformation with large-scale folding and granitoid intrusion (Vasil'ev et al., 1981; Kotov et al., 1997).

Conventional TIMS single-grain zircon dating of a syn-metamorphic hypersthene-bearing trondhjemite and two-pyroxene trondhjemites yielded ages of 489 ± 1 and 488.0 ± 0.5 Ma, whereas metamorphic zircons from a syn-metamorphic two-pyroxene trondhjemite (enderbite) yielded a concordant age of 478 ± 2 Ma (Salnikova et al., 1998). This age was interpreted as the time of the peak granulite-facies metamorphism in the Slyudyansky Complex. A post-metamorphic amphibole-two-pyroxene-quartz syenite has a concordant zircon age of 471 ± 2 Ma (Kotov et al., 1997; Salnikova et al., 1998) and a porphyritic plagioclase–microcline granite has a zircon age of 467 ± 3 Ma (Stepanov et al., 2009).

K–Ar ages of amphibole and diopside from rocks of the Slyudanskaya and Khangarulskaya "series" vary from 203 to 1481 Ma (Shafeev, 1970; Volobuev et al., 1980), and a whole-rock Pb–Pb isochron age for marbles of the Pereval'naya suite is 1980 ± 60 Ma (Volobuev et al., 1980). $^{207}Pb/^{206}Pb$ ages for multigrain zircon fractions from the granulite-facies rocks show a large range from 400–600, 870–950, 1200–1300, 1500–1650, 1900–2100, to 2400 Ma (Vasil'ev and Reznitskiy, 1993). U–Pb dating of multigrain fractions of detrital and metamorphic zircons from clastic metasedimentary rocks yielded data with poor alignment along a discordia that intercepts Concordia at 556 ± 20 and 2630 ± 25 Ma (Reznitskii et al., 1991). All these data reveal a complicated geological evolution of the Slyudyansky Complex but failed in constraining the deposition ages of the supracrustal rocks.

SHRIMP zircon ages were recently obtained for detrital zircons from a quartzite layer intercalated with marbles of the Pereval'naya suite (Rudenko et al., 2007; Stepanov et al., 2009). The $^{207}Pb/^{206}Pb$ ages vary from 3000 to 3260 Ma, and only two metamorphic rims yielded ages of 1254 and 2409 Ma. Thus, the new data indicate an Archean crustal source and provide a lower limit for deposition of the quartzite. However, these data need to be confirmed by further dating of detrital zircons from other clastic sedimentary lithologies in the Slyudyansky Complex.

3. Analytical techniques

Major element abundances were analyzed using XRF methods in the Institute of the Earth's Crust, Siberian Branch, Russian Academy of Sciences (RAS), Irkutsk. The detailed analytical procedure are described in Afonin et al. (1992).

Trace elements and REE concentrations were determined by a VG Elemental PlasmaQuad PQ2+ "Turbo" inductively coupled plasma mass spectrometer (ICP-MS) after lithium metaborate fusion. Analytical procedures were described in detail by Panteeva et al. (2003). Standard reference materials were BHVO-2 (basalt), RGM-1 (ryolite), W-2 (diabase), JG-2 and G-2 (granites). The precisions for determined element results are better than 10%".

Zircon microphotographs were made in the Institute of Precambrian Geology and Geochronology (IPGG), Russian Academy of Sciences (IPGG RAS), St. Petersburg, using a Scanning Electron Microscope ABT-55 (accelerating voltage 15 kV). Cathodoluminescence (CL) images of zircons were taken using a panchromatic CL imaging system (Gatan Mini-CL) attached to a scanning electron microscope JOEL JSM-6360LV at the Institute of Earth Sciences, Academia Sinica, Taipei, for examining the internal structures of zircon grains and selecting optimum spot locations for in situ U–Pb dating and Hf isotopic analysis. The Hf analyticat spot was place on top of the spot previously analyzed for U–Pb assuming that the zircon does not have latheral and vertical zoning within several tens of microns.

Sm–Nd isotopic analyses were performed at the IPGG. About 100 mg of whole rock powder was dissolved in a mixture of HF, HNO_3 and $HClO_4$. A ^{149}Sm–^{150}Nd spike solution was added to all samples before dissolution. REE were separated on BioRad AGW50-X8 200–400 mesh resin using conventional cation-exchange techniques. Sm and Nd were separated by extraction chromatography with a LN-Spec (100–150 mesh) resin. The total blank in the laboratory was 0.1–0.2 ng for Sm and 0.1–0.5 ng for Nd. Isotopic compositions of Sm and Nd were determined on a Finnigan MAT-261 and a TRITON TI multicollector mass-spectrometer, both in static mode. The precision (2σ) of Sm and Nd contents and $^{147}Sm/^{144}Nd$ ratios was ca. 0.5% and ca. 0.005% for $^{143}Nd/^{144}Nd$ ratios. $^{143}Nd/^{144}Nd$ ratios were adjusted relative to the value of 0.511860 for the La Jolla standard. During the period of analysis the weighted average of 9 La Jolla Nd standard runs yielded 0.511852 ± 8 (2σ) for $^{143}Nd/^{144}Nd$, normalized against $^{146}Nd/^{144}Nd = 0.7219$.

The $\varepsilon_{Nd}(t)$ values were calculated using the present-day values for a chondritic uniform reservoir (CHUR) $^{143}Nd/^{144}Nd = 0.512638$ and $^{147}Sm/^{144}Nd = 0.1967$ (Jacobsen and Wasserburg, 1984). Whole-rock Nd t_{DM} mean crustal residence ages were calculated

using the model of Goldstein and Jacobsen (1988) according to which the Nd isotopic composition of the depleted mantle evolved linearly since 4.56 Ga ago and has a present-day value $\varepsilon_{Nd}(0)$ of +10 ($^{143}Nd/^{144}Nd$ = 0.513151 and $^{147}Sm/^{144}Nd$ = 0.2137). Two-stage Nd model ages t_{DM2} (Keto and Jacobsen, 1987) were calculated using a mean crustal ratio $^{147}Sm/^{144}Nd$ of 0.12 (Taylor and McLennan, 1985).

Zircon U–Pb isotopic data were obtained using the LA-ICP-MS technique at the Department of Geosciences, National Taiwan University, Taipei. An Agilent 7500s quadrupole ICP-MS and a NewWave UP213 laser ablation system were used, and the detailed analytical procedures can be found in Chiu et al. (2009). Laser ablation was performed with helium carrier gas that substantially reduces deposition of ablated material onto the sample surface and greatly improves transport efficiency, thus increasing the signal intensity as compared to "conventional" ablation using argon as the carrier gas (Eggins et al., 1998; Günther and Heinrich, 1999; Jackson et al., 2004). During the experiments, about 1 min was spent for measuring the gas blank, and the results indicate a sensitivity of less than 1000 counts per second (cps) for all measured isotopes. Calibration was performed using the GJ-1 zircon standard, with a well established precise $^{207}Pb/^{206}Pb$ age and an intercept age, using isotope dilution thermal ionization mass spectrometry (ID-TIMS), of 608.5 ± 0.4 Ma (2σ) and 608.5 ± 1.5 Ma (2σ), respectively (Jackson et al., 2004). The Harvard reference zircon 91500 and Australian Mud Tank carbonatite zircon (MT) were used

Table 1
Major and trace element composition of the gneisses from the Slyudyansky Complex.

No	1	2	3	4	5	6	7	8	9	10
Sample no	BS-137	BS-142	BS-198	BS-372	Kh-253	BS-56	PS-9b (PS-10)	PS-81	PS-365 (PS-386)	PS-387
SiO_2	60.76	63.78	57.10	60.24	62.62	61.94	62.36	60.37	58.59	60.64
TiO_2	0.84	0.66	0.89	0.96	0.86	0.86	0.73	0.89	0.95	0.69
Al_2O_3	17.39	16.42	14.90	18.31	14.87	17.84	14.15	16.50	16.37	16.15
Fe_2O_3	3.31	2.06	2.38	2.71	3.43	1.95	1.31	1.12	1.74	1.36
FeO	4.16	5.53	9.90	5.12	5.31	8.05	8.09	8.26	7.96	4.71
MnO	0.10	0.16	0.41	0.23	0.12	0.18	0.08	0.18	0.20	0.06
MgO	2.26	2.26	6.32	3.02	4.09	3.46	7.67	3.47	3.55	2.20
CaO	3.14	4.19	1.44	1.12	2.53	0.18	1.54	5.13	6.58	4.66
Na_2O	3.38	1.79	1.48	2.13	2.08	1.35	0.54	2.64	2.26	3.62
K_2O	2.08	1.13	2.56	3.70	2.50	1.08	1.70	0.98	0.31	3.46
P_2O_5	0.06	0.10	0.05	0.06	0.11	0.01	0.13	0.22	0.23	0.47
LOI	2.87	1.61	2.18	1.65	1.30	1.80	1.99	0.18	1.38	1.61
Total	100.35	99.69	99.61	99.25	99.82	98.70	100.29	99.94	100.12	99.63
D(F)	0.7	−2.3	−7.7	−2.2	−3.9	−6.8	−10.9	−1.8	−1.7	3.1
CIA	62.0	67.3	69.6	68.2	63.8	83.4	77.4	62.1	62.0	53.7
CIW	67.4	70.9	79.9	80.2	72.2	88.2	86.1	64.7	62.8	61.3
Sc	13.8	16.8	24	11.3	2.6	14.6	24		19	8.6
V	165	219	139	95	140	112	233		171	85
Cr	44	25	187	33	98	114	445		124	27
Co	29	21	44	18.2	25	40	51		28	18.2
Ni	45	20	288	41	65	217	389		57	27
Cu	52	14.5	42	51	3.0	55	29		30	44
Zn	121	85	221	72	83	141	121		123	73
Ga	23	21	22	13.4	15.4	17.1	24		23	21
Rb	83	57	74	45	10.6	48	70		2.7	71
Sr	251	328	121	122	120	50	55		622	448
Y	17.7	18.5	39	17.4	16.5	26	26		28	10.2
Zr	53	101	69	29	50	45	117		106	34
Nb	14.1	11.1	18.3	9.5	11.0	11.7	10.1		11.7	5.3
Ba	204	485	1338	275	480	990	590		132	2002
La	37	25	48	25	13.8	27	31		26	39
Ce	77	50	98	54	31	60	67		55	75
Pr	8.9	6.1	11.0	6.2	3.9	6.6	7.4		7.1	9.0
Nd	32	21	38	23	15.8	25	27		28	35
Sm	5.8	4.1	6.6	4.6	3.3	4.5	5.0		5.3	5.2
Eu	1.21	1.02	1.28	1.01	0.88	1.04	0.97		1.60	2.4
Gd	5.7	4.2	6.3	4.3	3.6	4.3	4.7		5.7	5.1
Tb	0.63	0.57	0.85	0.53	0.54	0.70	0.60		0.76	0.49
Dy	3.3	3.0	5.9	2.8	3.2	4.3	3.8		4.5	2.1
Ho	0.58	0.69	1.39	0.62	0.66	0.84	0.83		0.90	0.36
Er	1.77	1.67	3.6	1.75	1.89	2.2	2.5		2.5	0.70
Tm	0.29	0.30	0.63	0.34	0.34	0.40	0.42		0.42	0.12
Yb	1.89	1.68	3.8	2.0	1.71	2.6	2.7		2.7	0.69
Lu	0.29	0.27	0.67	0.31	0.28	0.40	0.41		0.41	0.12
Hf	1.45	2.5	1.59	0.70	1.26	1.12	2.9		2.3	0.76
Ta	0.48	0.64	0.49	0.41	0.57	0.45	0.46		0.60	0.13
Pb	14.5	9.5	6.8	12.5	7.3	14.9	8.8		7.9	9.3
Th	10.9	6.9	16.0	6.5	3.6	8.2	9.4		8.0	0.28
U	0.96	0.99	0.78	0.75	1.00	0.69	1.87		1.52	0.06
$(La/Yb)_N$	13.3	10.0	8.4	8.2	5.5	7.0	7.7		6.6	38.1
$(La/Sm)_N$	4.0	3.9	4.6	3.4	2.6	3.9	3.9		3.1	4.7
$(Gd/Yb)_N$	2.4	2.0	1.3	1.7	1.7	1.3	1.4		1.7	5.9
Eu/Eu^*	0.63	0.74	0.60	0.68	0.77	0.71	0.60		0.88	1.40

Notes. Samples 1–5 – gneisses of the Khangarulskaya "series" formation, 6–11 – gneisses of the Slyudyanskaya "series". Sample PS-365 is analog of the sample PS-386 used for U–Pb and Hf isotope zircon investigations. D(F) – index D. Shaw (1986). CIA – index of chemical weathering. Paragenesis: BS-137 – grt-bt-sill; BS-142 – grt-bt; BS-198 – bt-grt-hy-crd; BS-372 – grt-bt-sil-crd; Kh-253 – bt-grt; BS-56 – bt-grt-crd; PS-9b (PS-10) – bt-grt-hy-crd; PS-81 – grt-hy-bt; PS-365 (PS-386) – bt-grt-hy; PS-387 – bt-2px.

as secondary standards for data quality control. All U–Th–Pb isotopic ratios were calculated using the GLITTER 4.0 (GEMOC) software, and common lead was corrected using the common lead correction function proposed by Anderson (2002). Weighted mean U–Pb ages and concordia plots were calculated using Isoplot v. 3.0 (Ludwig, 2003). Our $^{207}Pb/^{235}U$, $^{206}Pb/^{238}U$ and $^{207}Pb/^{206}Pb$ ages of zircon 91500 are 1061.8 ± 2.1 Ma (2σ), 1062.1 ± 1.7 Ma (2σ) and 1066.7 ± 2.1 Ma (2σ), respectively, which are in excellent agreement with the consensus values reported by Wiedenbeck et al. (1995) using ID-TIMS methods. Our $^{207}Pb/^{235}U$, $^{206}Pb/^{238}U$ and $^{207}Pb/^{206}Pb$ ages of zircon MT are 736.8 ± 5.2 Ma (2σ), 734.0 ± 2.4 Ma (2σ) and 739.2 ± 8.1 Ma (2σ), respectively, and also match the U–Pb concordia intercept age of 732 ± 5 Ma recommended by Black and Gulson (1978). For the "best zircon age" in Table 3, we follow Black and Jagodzinski (2003) and quote the $^{206}Pb/^{238}U$ age for zircons younger than 1000 Ma and the $^{207}Pb/^{206}Pb$ age for older zircons.

In situ Hf isotope analyses were carried out using a New Wave UP 213 laser-ablation microprobe, attached to a Nu Plasma multicollector ICP-MS, at the Institute of Earth Sciences, Academia Sinica, in Taipei. Instrumental conditions and data acquisition procedures follow that reported by Griffin et al. (2000). Masses 172, 175, 176, 177, 178, 179 and 180 were simultaneously analyzed, and all analyses were carried out in static-collection mode. Data were normalized to $^{179}Hf/^{177}Hf = 0.7325$, using an exponential correction for mass bias. Initial setup of the instrument was done using a 50 ppb solution of AMES Hf metal, which typically yielded a total Hf beam of 10–14 $\times$ 10^{-11} A. Isobaric interference of ^{176}Lu and ^{176}Yb on ^{176}Hf was corrected by measuring the intensities of the interference-free ^{175}Lu and ^{172}Yb isotopes and using appropriate $^{176}Lu/^{175}Lu$ and $^{176}Yb/^{172}Yb$ to calculate $^{176}Lu/^{177}Hf$ and $^{176}Yb/^{177}Hf$. As the analytical method is similar to that reported by Griffin et al. (2000), the recommended $^{176}Lu/^{175}Lu$ and $^{176}Yb/^{172}Yb$ ratios of 0.02669 (De Biévre and Taylor, 1993) and 0.5865 were used for data reduction. The reproducibility of our Hf isotopic analysis is demonstrated by 28 Hf analyses on the 50 ppb solution of the AMES Hf metal since March 2007, covering the period of laser-ablation analyses reported here. Our mean value for $^{176}Hf/^{177}Hf$ is 0.282152 ± 18 (2σ), which is identical to the recommended value of 0.282151 ± 13 by Münker et al. (2001). The typical 2σ uncertainty on a single analysis of $^{176}Hf/^{177}Hf$ is 6–8 $\times$ 10^{-6}.

The New Wave UP 213 laser system delivers a beam of 213 nm UV light from a frequency-quintupled (5th harmonic) Nd: YAG laser. Most analyses were carried out with a beam diameter of 55 μm, 5 Hz repetition rate, and energies of ~0.4 mJ/pulse. This resulted in total Hf signals of 1–2.5 $\times$ 10^{-11} A, depending on precise conditions and the Hf contents. Typical ablation times were 80–120 s. The He carrier gas transported the ablated sample from the laser-ablation cell via a mixing chamber where it was mixed with Ar prior to entering the ICP-MS torch. Flux rate for He was about 1 l/min and 0.7 l/min for Ar. The laser-ablation analyses were carried out using the time-resolved analysis software, in which the signal for each mass and each ratio is displayed as a function of time during the analysis. This allows the more stable portions of the ablation to be selected for analysis, before the data are processed to give the final results. The background noise was collected for 30 s before ablation began. Typical within-run precision (2σ) on the analysis of $^{176}Hf/^{177}Hf$ is ±0.000030, equivalent to an uncertainty of ~1 epsilon unit.

To evaluate the accuracy and precision of the laser-ablation results, we repeatedly analyzed two zircon standards, Mud Tank and 91500. Both have been described by Woodhead and Hergt (2005), Griffin et al. (2006), and Wiedenbeck et al. (1995). Our long-term result of the Mud Tank zircon gave $^{176}Hf/^{177}Hf = 0.282518 \pm 48$ (2σ; $n = 65$), which is consistent with the value of 0.282522 ± 42 (2σ; $n = 2335$) reported by Griffin et al. (2006) and the values given by Woodhead and Hergt (2005) for solution (0.282507 ± 6; $n = 5$) and LAM-MC-ICP-MS analyses (0.282504 ± 44; $n = 158$). Our mean result for 91500 is 0.282319 ± 94 (2σ; $n = 28$), which is also similar to the literature values but shows a large spread of the data. Griffin et al. (2006) pointed out the isotopic heterogeneity of 91500, so it may not be a suitable standard for evaluation of the precision and accuracy of in situ analysis. In any case, our Mud Tank results demonstrate the reliability of the zircon Hf isotope analyses.

To calculate $\varepsilon_{Hf}(t)$ values, we adopted the chondritic ratios of $^{176}Hf/^{177}Hf$ (0.282772) and $^{176}Lu/^{177}Hf$ (0.0332) given by Blichert-Toft and Albarède (1997). These values were reported relative to $^{176}Hf/^{177}Hf = 0.282163$ for the JMC475 standard. The $^{176}Hf/^{177}Hf$ value of 0.282152 ± 18 was obtained for our AMES Hf metal, which is isotopically indistinguishable from the JMC475 standard. To calculate $\varepsilon_{Hf}(t)$ values and depleted mantle Hf model ages $t_{Hf(DM)}$ we used the weighted average or Concordia ages for concordant zircons and $^{207}Pb/^{206}Pb$ apparent ages for discordant zircons and applied the ^{176}Lu–^{176}Hf decay constants proposed by Scherer et al. (2001) and the CHUR and DM parameters of Blichert-Toft and Albarède (1997) and Griffin et al. (2000, 2004). The zircon Hf "crustal" model age t_{Hfc} is based on a depleted-mantle source and the assumption that the protolith of the zircon's host magma had the isotopic composition of average continental crust, namely a $^{176}Lu/^{177}Hf$ ratio of 0.0093 (Amelin et al., 1999). If a higher crustal $^{176}Lu/^{177}Hf$ ratio of 0.015 is used (Griffin et al., 2002), unrealistically high t_{Hfc} values up to 4.3 Ga are calculated, and we therefore consider the value of 0.0093 to most closely reflect crustal compositions in our study region.

4. Results

4.1. Geochemical and Nd isotopic data

Paragneiss samples of the Slyudyansky Complex are characterized by intermediate SiO_2 (57–64 wt.%), low alkalinity ($Na_2O + K_2O$ = 2.24–5.83 wt.%) and variable Na_2O/K_2O ratios of 0.32–7.29 (Table 1). They mostly have a negative index D, Shaw (Shaw, 1970) D(x) from 0.7 to −10.9, and index of chemical alteration CIA = 62–83, and correspond to graywacke of intermediate composition. The biotite-two-pyroxene gneisses display higher alkalinity ($Na_2O + K_2O$ = 7.08–7.45 wt.%), positive D(x) values of 2.9–3.1, lower CIA = 53–54, and approach magmatic rocks such as quartz diorite in chemical composition.

The Slyudyansky Complex metagraywackes show negative Nb–Ta, P, Zr–Hf and Ti anomalies in primitive-mantle-normalized trace element variation diagrams (Fig. 4). The biotite-two pyroxene gneisses have low contents of Rb, Th, U and HREE, highly fractionated REE distributions ($La_N/Yb_N = 38$) with with HREE depletion (Yb = 0.69 ppm) and positive Eu anomaly ($Eu/Eu^* = 1.40$). Other gneisses are characterized by moderately fractionated REE patterns LREE enrichment (La_N/Yb_N = 5.5–13.0), flat to slightly fractionated HREE distribution (Gd_N/Yb_N = 1.3–2.4), and pronounced negative Eu anomalies (Eu/Eu^* = 0.60–0.77).

Gneisses of the Slyudyansky Complex have depleted mantle Nd model ages $t_{Nd(DM)}$ of 1.7–2.2 and 2.8–3.0 Ga, whereas crustal Nd model ages t_{Ndc} are 1.9–2.2 and 3.3 Ga (Table 2). The Mesoarchean Nd model ages are only characteristic of the biotite-two-pyroxene gneisses and suggest derivation of their protholiths from local sources different from sources of other Slyudyansky metagraywackes.

The geochemical features indicate derivation of the Slyudyansky metagraywackes from evolved crustal sources. However, these metagraywackes have high concentrations of Ba, Cr and Ni (Table 1), thus also suggesting an input from mafic–ultramafic

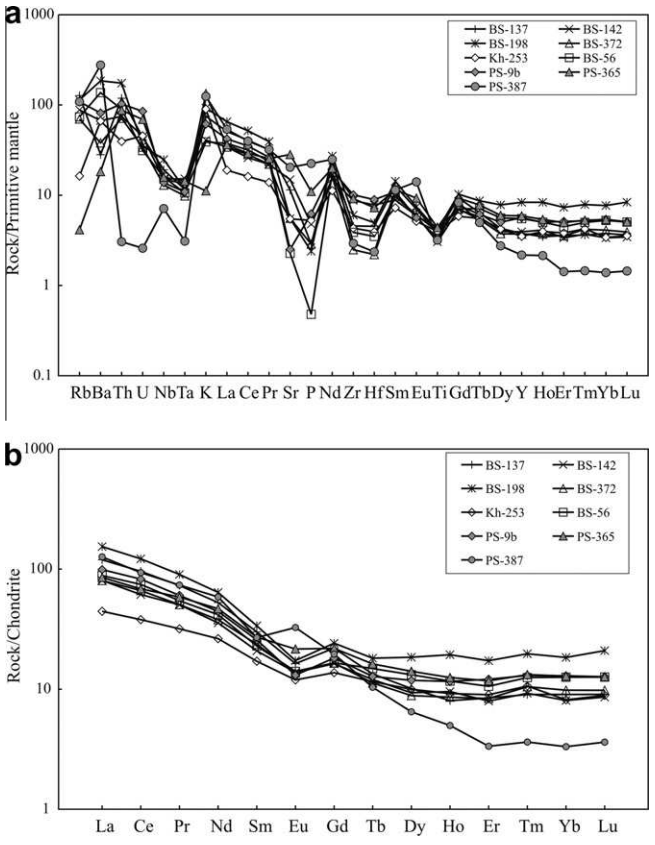

Fig. 4. (a) Primitive-mantle-normalized trace-element variation diagram, (b) chondrite-normalized REE distribution patterns in metasedimentary rocks of the Slyudyansky Complex.

sources (Petrova et al., 2002; Makrygina et al., 2007). This assumption is supported by Cr–V mineralization in Slyudyansky Complex marbles and quartzites (Reznitskii et al., 1988) and back arc basin geochemical signatures of Slyudyansky metabasalts (Makrygina et al., 2007). The Khangarulskaya "series" of the Slyudyansky Complex contain large volume of metatuffite of andesitic composition (Reznitskii et al., 2004). According to available geochemical data (Petrova et al., 2002, 2005; Makrygina et al., 2007) the sedimentary rocks of the Slyudyansky Complex were formed by erosion of granitic (granulite–gneissic) and mafic–ultramafic rocks in fore-arc (Khangarulskaya "series") and an ensialic bark-arc (Slyudyanskaya "series") basin setting.

4.2. Zircon ages

Zircons were separated from a biotite–garnet–hyperstene plagiogneiss (sample PS-386, an analog of sample PS-365 in Tables 1 and 2) and a biotite-two-pyroxene gneiss (sample PS-387) of the lower Kultukskaya suite. A total of 67 spots on 48 grains were analysed, and the analytical data are presented in Table 3. SEM photomicrographs of the dated zircons are presented in Fig. 5, and cathodoluminescence (CL) images of concordant and selected typical discordant zircons are shown in Fig. 6.

Detrital zircons in the analyzed samples are heterogeneous, and several typical "magmatic" and "metamorphic" subtypes can be distinguished according to their morphology, CL images and U–Pb isotopic data. The type considered to be of metamorphic origin makes up about 10% of the bulk population and consists of transparent or semitransparent subhedral, short-prismatic to isometric (sample No PS-386) or irregular-shaped (sample No PS-387), brown to pink grains with a length/width ratio of 1.2–2.0 (Fig. 5a–d). These zircons have very dark or dark-gray luminescene and are cloudy and diffuse under CL (Fig. 6a–f). Some grains of this type from sample PS-387 exhibit relicts of oscillatory zoning and contain dark cores, presumably inherited (Fig. 6g–j). Morphological features and the internal structure of these zircons suggest a high-grade metamorphic origin. Zircons from the biotite–garnet–hyperstene (Fig. 5a–c) and biotite-two-pyroxene gneisses (Fig. 6e–j) are concordant and have weighted mean $^{206}Pb/^{238}U$ ages of 488 ± 10 Ma (MSWD = 0.19, probability = 0.90; $n = 4$) and 486 ± 8 Ma (MSWD = 0.28, probability = 0.93; $n = 6$) respectively (Figs. 7a and b). Only one grain of sample PS-387 (No. 37 in Table 3) yielded a younger $^{206}Pb/^{238}U$ age of 458 ± 10 Ma. If all data are pooled, this type of zircon provides weighted mean $^{206}Pb/^{238}U$ ages of 487 ± 6 Ma (MSWD = 0.23, probability = 0.99; $n = 10$) and 458 ± 10 Ma (Fig. 7c). Two inherited cores with relict oscillatory (magmatic) zoning are strongly discordant and have minimum $^{207}Pb/^{206}Pb$ ages of 2299 ± 28 and 2126 ± 30 Ma (Nos. 51 and 64 in Table 3).

An optically distinctive type of zircon makes up about 40% of the population in biotite–garnet–hyperstene plagiogneiss sample PS-386 but is rare in sample PS-387 of the biotite-two-pyroxene gneiss. It consists of transparent or semitransparent, subhedral to euhedral, prismatic or bipyramidal (Fig. 5e–f) pale-pink, magmatically zoned crystals containing inherited and partially recrystallized cores with cloudy, diffuse CL images of medium intensity. Narrow and brightly luminescent (low-U) rims were detected on these grains (Figs. 6k–r). Seven spots representing the zoned interior yielded three clusters of concordand ages (Fig. 7d), namely 691 ± 20 Ma ($n = 2$, MSWD = 0.19, probability = 0.66), 774 ± 24 ($n = 2$, MSWD = 0.0017, probability = 0.97), and 825 ± 20 ($n = 3$, MSWD = 0.088, probability = 0.92). It is evident from the morphological features and internal structures of these zircons that they are of likely magmatic origin, and the ages therefore reflect the times of zircon crystallization from melts.

The dominant zircon type in biotite-two-pyroxene–plagioclase gneiss sample PS-387 consists of semitransparent or transparent, subhedral, pale-pink prismatic or oval grains with a length/width

Table 2
Sm–Nd isotopic compositions of the gneisses from the Slyudyansky Complex.

Sample	Sm, ppm	Nd, ppm	$^{147}Sm/^{144}Nd$	$^{143}Nd/^{144}Nd$, ±2σm	$\varepsilon_{Nd}(0)$	$\varepsilon_{Nd}(t)$	$t_{Nd(DM)}$, Ma	t_{Ndc}, Ma
BS-137	5.73	31.3	0.1110	0.511977 ± 8	−12.9	−7.6	1737	1857
BS-142	3.82	19.80	0.1171	0.511897 ± 10	−14.5	−9.5	1973	2018
BS-198	6.98	39.6	0.1067	0.511843 ± 9	−15.5	−9.9	1858	2051
BS-372	6.07	31.0	0.1189	0.511954 ± 8	−13.3	−8.5	1919	1935
Kh-253	4.30	21.4	0.1222	0.511922 ± 11	−14.0	−9.3	2041	2004
BS-56	5.85	32.6	0.1091	0.511791 ± 10	−16.5	−11.1	1974	2147
PS-9b	4.16	22.1	0.1141	0.511775 ± 8	−16.8	−11.7	2098	2199
PS-365	5.26	25.4	0.1255	0.511894 ± 10	−14.5	−10.1	2164	2066
PS-387	5.24	32.9	0.0965	0.511005 ± 10	−31.9	−25.6	2775	3343
PS-387A	5.46	31.0	0.1065	0.511041 ± 5	−31.2	−25.6	2980	3336

Notes. $\varepsilon_{Nd}(t)$ and t_{Ndc} values calculated on the age of the granulite facies metamorphism ca. 488 Ma.

Table 3
Analytical data of U–Pb dating of zircons from metasedimentary of the Slyudyansky Complex.

No	Analysis	Corrected ratios						Rho	Corrected ages, Ma								Th/U	Comments
		$^{207}Pb/^{206}Pb$	1σ	$^{207}Pb/^{235}U$	1σ	$^{206}Pb/^{238}U$	1σ		$^{207}Pb/^{206}Pb$	1σ	$^{207}Pb/^{235}U$	1σ	$^{206}Pb/^{238}U$	1σ	$^{208}Pb/^{232}Th$	1σ		
Biotite–garnet–hyperstene plagiogneiss PS-386																		
1	PS-386-01-1	0.0910	0.0028	2.2145	0.1150	0.1765	0.0045	0.49	1447	54	1186	36	1048	24	1025	24	0.53	Core NP
2	PS-386-01-2	0.0671	0.0007	1.2714	0.0290	0.1375	0.0030	0.90	840	20	833	13	830	17	885	21	0.14	
3	PS-386-02	0.0566	0.0005	0.6087	0.0131	0.0780	0.0017	0.90	478	23	483	8	484	10	530	13	0.012	
4	PS-386-03	0.0567	0.0005	0.6132	0.0132	0.0785	0.0017	0.90	478	22	486	8	487	10	548	12	0.027	
5	PS-386-04	0.1189	0.0029	3.7895	0.1667	0.2312	0.0058	0.57	1939	43	1591	35	1341	30	1298	31	0.49	Core NP
6	PS-386-05-1	0.1722	0.0027	9.2871	0.3280	0.3911	0.0098	0.71	2580	26	2367	32	2128	45	2076	48	0.66	Core NP
7	PS-386-05-2	0.0671	0.0007	1.2540	0.0281	0.1356	0.0029	0.90	840	20	825	13	820	17	861	18	0.55	
8	PS-386-06-1	0.0924	0.0012	1.7860	0.0569	0.1402	0.0034	0.77	1476	23	1040	21	846	19	818	20	0.22	
9	PS-386-06-2	0.1402	0.0028	6.0897	0.2490	0.3150	0.0080	0.62	2230	35	1989	36	1765	39	1721	40	0.79	Core NP
10	PS-386-07-1	0.1587	0.0031	6.5425	0.2476	0.2990	0.0070	0.62	2442	32	2052	33	1687	35	1619	35	0.75	Core NP
11	PS-386-07-2	0.0682	0.0008	1.2804	0.0347	0.1363	0.0030	0.81	873	26	837	15	824	17	874	20	0.62	
12	PS-386-07-3	0.0666	0.0008	1.0396	0.0280	0.1132	0.0025	0.82	825	26	724	14	691	14	778	18	0.57	
13	PS-386-08	0.1200	0.0016	3.2891	0.0972	0.1987	0.0044	0.74	1957	23	1478	23	1169	23	1120	23	0.39	Core NP
14	PS-386-09	0.0578	0.0006	0.6249	0.0150	0.0784	0.0017	0.90	523	22	493	9	487	10	1137	28	0.056	
15	PS-386-10-1	0.1334	0.0025	5.5706	0.2095	0.3029	0.0072	0.63	2143	32	1912	32	1706	35	1666	37	0.61	Edge
16	PS-386-10-2	0.1457	0.0027	8.3370	0.3191	0.4150	0.0099	0.62	2296	30	2268	35	2238	45	2231	48	0.88	Centre
17	PS-386-11	0.3053	0.0039	22.9639	0.7577	0.5456	0.0142	0.79	3497	19	3225	32	2807	59	2703	65	0.93	
18	PS-386-12	0.1702	0.0033	10.9980	0.4556	0.4688	0.0126	0.65	2559	29	2523	39	2478	55	2467	60	0.95	
19	PS-386-13-1	0.1376	0.0021	3.3619	0.1065	0.1772	0.0039	0.69	2197	26	1496	25	1052	21	988	21	0.48	Core NP
20	PS-386-13-2	0.0639	0.0006	1.0037	0.0223	0.1139	0.0025	0.90	739	22	706	11	695	14	759	16	0.42	
21	PS-386-14	0.3179	0.0031	31.7848	0.6886	0.7251	0.0159	0.90	3560	13	3544	21	3515	59	3702	74	0.98	
22	PS-386-15-1	0.2154	0.0022	11.8884	0.2726	0.4003	0.0093	0.90	2947	17	2596	21	2171	43	2157	47	0.16	Edge
23	PS-386-15-2	0.3017	0.0031	26.1011	0.5997	0.6276	0.0145	0.90	3479	17	3350	22	3140	58	3225	68	0.40	Core
24	PS-386-16-1	0.1426	0.0014	6.2419	0.1505	0.3176	0.0075	0.90	2259	18	2010	21	1778	37	1732	40	0.076	Core NP
25	PS-386-16-2	0.0634	0.0007	0.9808	0.0245	0.1122	0.0026	0.90	722	23	694	13	686	15	769	20	0.13	
26	PS-386-17	0.2208	0.0023	17.2125	0.3983	0.5656	0.0132	0.90	2986	17	2947	22	2890	54	2956	62	0.75	
27	PS-386-18-1	0.1224	0.0057	5.3969	0.3900	0.3198	0.0097	0.42	1991	85	1884	62	1789	47	1769	46	1.28	Edge
28	PS-386-18-2	0.2797	0.0029	21.7827	0.4989	0.5649	0.0131	0.90	3361	17	3174	22	2887	54	2939	62	0.41	Core
29	PS-386-19-1	0.1442	0.0013	5.5596	0.1316	0.2797	0.0064	0.90	2278	17	1910	20	1590	32	1532	34	0.080	Core NP
30	PS-386-19-2	0.0653	0.0007	1.1487	0.0277	0.1275	0.0030	0.90	785	23	777	13	774	17	793	19	0.15	
31	PS-386-20	0.0569	0.0006	0.6252	0.0144	0.0798	0.0018	0.90	486	24	493	9	495	11	506	13	0.025	
32	PS-386-21-1	0.1658	0.0032	8.8076	0.3892	0.3852	0.0111	0.65	2516	35	2318	40	2101	52	2054	55	0.81	Core NP
33	PS-386-21-2	0.1756	0.0018	9.8902	0.2247	0.4086	0.0094	0.90	2612	18	2425	21	2208	43	2281	48	0.56	Core NP
34	PS-386-21-3	0.0660	0.0007	1.1599	0.0286	0.1274	0.0030	0.90	807	22	782	13	773	17	820	20	0.22	
35	PS-386-22-1	0.1642	0.0017	7.7128	0.1752	0.3406	0.0078	0.90	2500	17	2198	20	1890	38	1900	41	0.31	Core NP
36	PS-386-22-2	0.0676	0.0007	1.2145	0.0306	0.1303	0.0030	0.90	857	22	807	14	790	17	834	23	0.12	
Biotite-two-pyroxene gneiss PS-387																		
37	PS-387-01	0.0566	0.0006	0.5742	0.0127	0.0736	0.0017	0.90	477	23	461	8	458	10	474	10	0.18	
38	PS-387-02	0.1515	0.0015	6.3289	0.1422	0.3030	0.0069	0.90	2363	18	2022	20	1706	34	1737	36	0.92	
39	PS-387-03	0.1528	0.0027	6.8445	0.2526	0.3248	0.0079	0.66	2378	27	2092	33	1813	39	1759	40	0.78	
40	PS-387-04-1	0.0564	0.0006	0.6058	0.0134	0.0780	0.0018	0.90	466	23	481	8	484	10	614	13	0.086	
41	PS-387-04-2	0.0575	0.0006	0.6124	0.0136	0.0773	0.0017	0.90	509	21	485	9	480	10	571	13	0.089	
42	PS-387-05-1	0.1718	0.0017	9.5477	0.2092	0.4032	0.0090	0.90	2575	17	2392	20	2184	42	2270	47	0.70	Edge
43	PS-387-05-2	0.1791	0.0018	11.4178	0.2514	0.4625	0.0104	0.90	2644	17	2558	21	2451	46	2522	52	0.80	Centre
44	PS-387-06	0.1168	0.0012	2.8306	0.0715	0.1757	0.0041	0.90	1908	19	1364	19	1044	22	996	23	0.11	
45	PS-387-07-1	0.1674	0.0017	8.3936	0.1857	0.3637	0.0082	0.90	2532	16	2274	20	2000	39	2057	43	0.68	Centre
46	PS-387-07-2	0.1468	0.0035	5.6350	0.2535	0.2784	0.0071	0.57	2309	41	1921	39	1583	36	1522	35	0.85	Edge
47	PS-387-08	0.0846	0.0012	1.3642	0.0455	0.1170	0.0028	0.72	1306	28	874	20	713	16	691	16	0.21	
48	PS-387-09	0.1524	0.0022	7.5394	0.2494	0.3587	0.0087	0.74	2373	25	2178	30	1976	41	1934	44	0.53	
49	PS-387-10	0.1599	0.0028	7.0339	0.2918	0.3190	0.0091	0.69	2455	30	2116	37	1785	45	1721	46	0.73	
50	PS-387-11	0.1447	0.0035	6.4959	0.2881	0.3256	0.0082	0.57	2284	47	2045	39	1817	40	1771	41	0.95	
51	PS-387-12-1	0.1459	0.0023	5.7380	0.1921	0.2852	0.0067	0.71	2299	28	1937	29	1618	34	1559	35	0.50	Core Pz

(*continued on next page*)

Table 3 (*continued*)

No	Analysis	Corrected ratios						Rho	Corrected ages, Ma								Th/U	Comments
		$^{207}Pb/^{206}Pb$	1σ	$^{207}Pb/^{235}U$	1σ	$^{206}Pb/^{238}U$	1σ		$^{207}Pb/^{206}Pb$	1σ	$^{207}Pb/^{235}U$	1σ	$^{206}Pb/^{238}U$	1σ	$^{208}Pb/^{232}Th$	1σ		
52	PS-387-12-2	0.0597	0.0016	0.6490	0.0294	0.0788	0.0018	0.51	593	60	508	18	489	11	486	13	0.77	Rim
53	PS-387-13	0.1643	0.0016	7.0965	0.1531	0.3132	0.0067	0.90	2501	16	2124	19	1757	33	1764	37	0.53	
54	PS-387-14	0.1534	0.0021	6.8287	0.2195	0.3229	0.0077	0.74	2384	22	2089	28	1804	37	1748	39	0.56	
55	PS-387-15	0.1590	0.0031	7.6330	0.2994	0.3482	0.0086	0.63	2445	32	2189	35	1926	41	1872	43	0.72	
56	PS-387-16	0.0591	0.0009	0.6007	0.0207	0.0737	0.0017	0.67	572	33	478	13	458	10	455	10	0.20	
57	PS-387-17	0.0578	0.0010	0.6244	0.0214	0.0784	0.0018	0.66	521	34	493	13	487	11	486	11	0.034	
58	PS-387-18	0.1608	0.0022	8.1899	0.2595	0.3695	0.0082	0.70	2464	23	2252	29	2027	39	1979	41	0.61	
59	PS-387-19	0.1513	0.0025	6.9049	0.2479	0.3310	0.0080	0.68	2361	29	2099	32	1843	39	1792	40	0.63	
60	PS-387-20	0.1563	0.0026	7.0108	0.2565	0.3253	0.0080	0.67	2416	31	2113	33	1816	39	1758	40	0.70	
61	PS-387-21	0.1657	0.0021	8.5494	0.2627	0.3743	0.0088	0.77	2514	24	2291	28	2050	41	1999	44	0.62	
62	PS-387-22	0.1578	0.0018	7.4213	0.2228	0.3411	0.0081	0.79	2432	21	2164	27	1892	39	1837	41	0.47	
63	PS-387-23	0.1509	0.0015	5.6346	0.1211	0.2709	0.0058	0.90	2356	16	1921	19	1545	29	1567	33	0.67	
64	PS-387-24-1	0.1321	0.0022	3.9125	0.1294	0.2149	0.0043	0.61	2126	30	1616	27	1255	23	1197	22	0.75	Core Pz
65	PS-387-24-2	0.0584	0.0007	0.6429	0.0165	0.0799	0.0017	0.84	543	25	504	10	495	10	536	31	0.040	Rim
66	PS-387-25	0.0571	0.0007	0.6117	0.0173	0.0777	0.0017	0.77	495	28	485	11	483	10	507	14	0.21	
67	PS-387-26	0.1156	0.0017	2.5664	0.0864	0.1610	0.0038	0.71	1890	28	1291	25	962	21	915	21	0.28	

Notes. Core NP – cores of the Neoproterozoic zircons.

ratio of 2–3 (Fig. 5g–j). This type also makes up about 50% of the bulk population in garnet–biotite–pyroxene gneiss sample PS-386. CL images show that many grains have a core with very different and discordant CL features. Overprinted magmatic zoning is found as well as bright or gray luminescent, unzoned metamorphic overgrowth (Fig. 6s–x). Th/U ratios in grains with oscillatory zoning vary from 0.12 to 0.95. Two crystals (Nos. 16 and 18 in Table 3) and one core (No. 26 in Table 3) from garnet–biotite–pyroxene plagiogneiss PS-386 are characterized by magmatic zoning (Fig. 6s–u). These yielded slightly discordant (3–4.0% of discordance) ages of 2262 ± 68 Ma (MSWD = 0.73, probability = 0.39), 2520 ± 77 Ma (MSWD = 1.13, probability = 0.29) and 2973 ± 29 Ma (MSWD = 2.6, probability = 0.11) (Fig. 7e). One rounded core with clear magmatic zoning (Fig. 6y) has a concordia age of 3555 ± 27 Ma (MSWD = 0.48, probability = 0.49) These ages are in agreement with $^{207}Pb/^{206}Pb$ ages of 3361 ± 17 to 3479 ± 17 Ma (Table 3, Fig. 7e) obtained for dark, inherited cores with relicts of magmatic zoning.

Other zircons and cores are discordant (from 11.6% to 56.4% of discordance) and provided a wide range of minimum $^{207}Pb/^{206}Pb$ ages from 1939 ± 43 to 2612 ± 18 Ma (Table 3). Cores of 825 ± 20 Ma old zircons are aligned along a discordia with an upper Concordia intercept at 2774 ± 100 Ma and lower intercept at 920 ± 84 Ma (MSWD = 1.2, probability = 0.27). In contrast, cores of 774 ± 24 Ma zircons are aligned along a discordia with intercepts at 2754 ± 81 and 954 ± 140 Ma (MSWD = 0.74, probability = 0.48) (Fig. 7f). All cores plotted together define a discordia with intercepts at 2747 ± 52 and 912 ± 82 Ma (MSWD = 0.68, probability = 0.60). The core of a 691 ± 20 Ma zircon has a Paleoproterozoic age of 2197 ± 26 that is close to ages of 2278 ± 17 and 2259 ± 18 Ma in zircon cores with low Th/U of 0.076–0.080 (Table 3). Another group of cores and zircons with Th/U of 0.57–0.77 define a discordia with intercepts at 2313 ± 72 and 608 ± 56 Ma (MSWD = 1.02, probability = 0.40) (Fig. 7g). All these ages cannot be related to distinct geological event but reflect zircon growth at ca. 2.3 and 2.8–2.7 Ga.

The discordant zircons as well as the inherited cores of sample PS-387 define a poor discordia (MSWD = 3.4) with intercepts at 2613 ± 39 and 639 ± 54 Ma (Fig. 7h). No Meso- or Paleoarchean zircons ages were found in this sample, and the oldest $^{207}Pb/^{206}Pb$ age is 2644 ± 17 Ma (Table 3). This may suggest that the main magmatic and probably metamorphic events in the source area(s) occurred in the Neoarchean at ca. 2.6–2.7 Ga.

Note that the magmatic zircons and cores with minimum $^{207}Pb/^{206}Pb$ ages of ca. 1.5 and 1.9 Ga are strongly discordant, and the data points are mainly distributed in the lower part of the Concordia diagram (Fig. 7). Only one zircon (No. 27, Table 3) with "granulitic" internal structure but high Th/U = 1.3 shows an older minimum $^{207}Pb/^{206}Pb$ age of 1991 ± 85 Ma (11.6% of discordance). These data suggest that the Meso- and Paleoproterozoic "ages" of ca. 1.5 and 1.9 Ga do not correspond to real magmatic or metamorphic events but either reflect Pb loss at unspecified times, perhaps in the Neoproterozoic or early Paleozoic, and/or are mixtures of Neoproterozoic and Neoarchean to Paleoproterozoic (ca. 2.7–2.3 Ga) zircon components.

4.3. Zircon Hf isotopic ratios

Thirty-six spots on 29 dated zircon grains were analyzed for their Lu/Hf isotopic composition, and the results are listed in Table 4. The $\varepsilon_{Hf}(t)$ data are plotted in Fig. 8.

Early Paleozoic (487 ± 6 Ma) zircons from biotite–garnet–hyperstene plagiogneiss PS-386 have negative $\varepsilon_{Hf}(t)$ values of −11.1 to −12.3 and Hf model ages $t_{Hf(DM)}$ of 1.5–1.6 Ga (t_{Hfc} = 1.8–1.9 Ga), whereas zircons of the same age from biotite-two-pyroxene plagiogneiss PS-387 yielded significantly lower

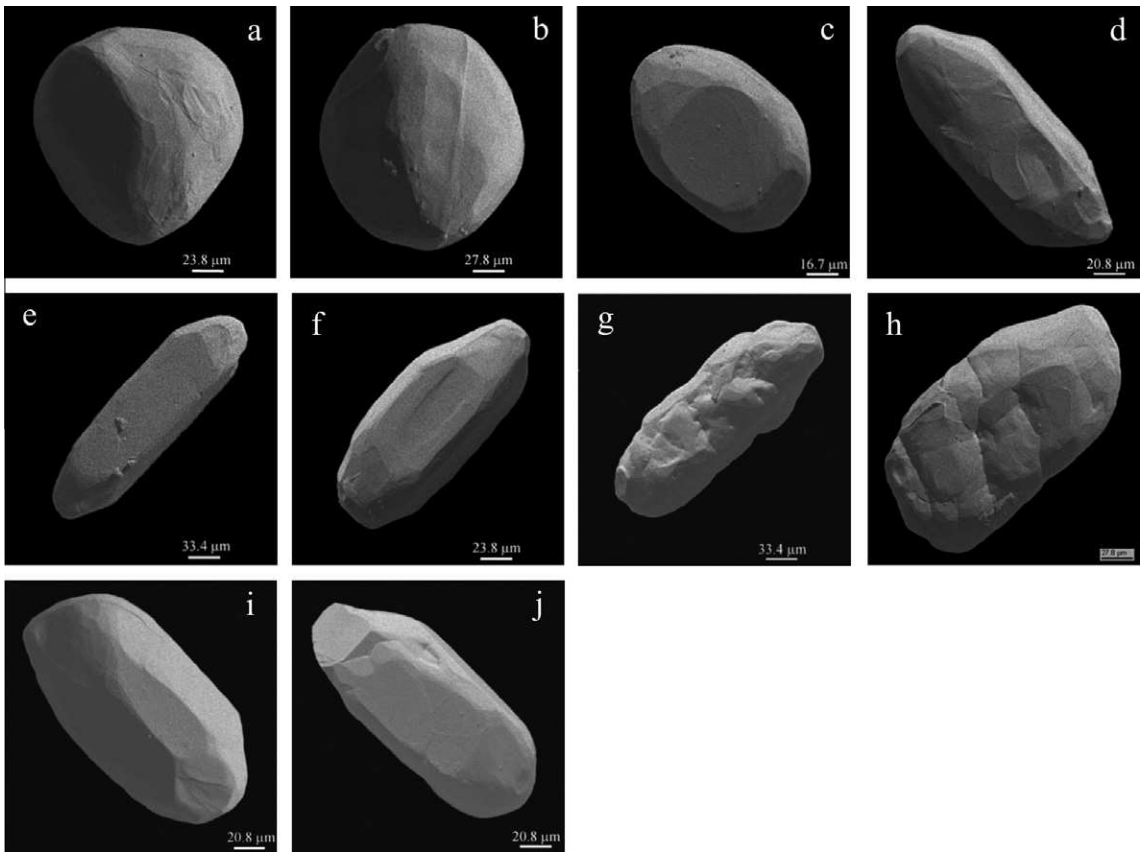

Fig. 5. SEM photomicrographs of dated zircons.

values $\varepsilon_{Hf}(t)$ values of −39.8 to −46.3 and older Hf model ages of 2.6–2.9 Ga (t_{Hfc} = 3.3–3.6 Ga). The 458 ± 10 Ma old zircons are characterized by $\varepsilon_{Hf}(t)$ values of −30.1 to −31.8 and $t_{Hf(DM)}$ of 2.2–2.3 Ga (t_{Hfc} = 2.8 Ga).

Neoproterozoic zircons also have negative $\varepsilon_{Hf}(t)$ values ranging from −9.1 to −10.4 for sample PS-386 ($t_{Hf(DM)}$ = 1.7 Ga, t_{Hfc} = 2.0 Ga) and from −16.3 to −21.3 for sample PS-386 ($t_{Hf(DM)}$ = 2.0–2.2 Ga, t_{Hfc} = 2.4–2.6 Ga). Meso- and Paleoarchean

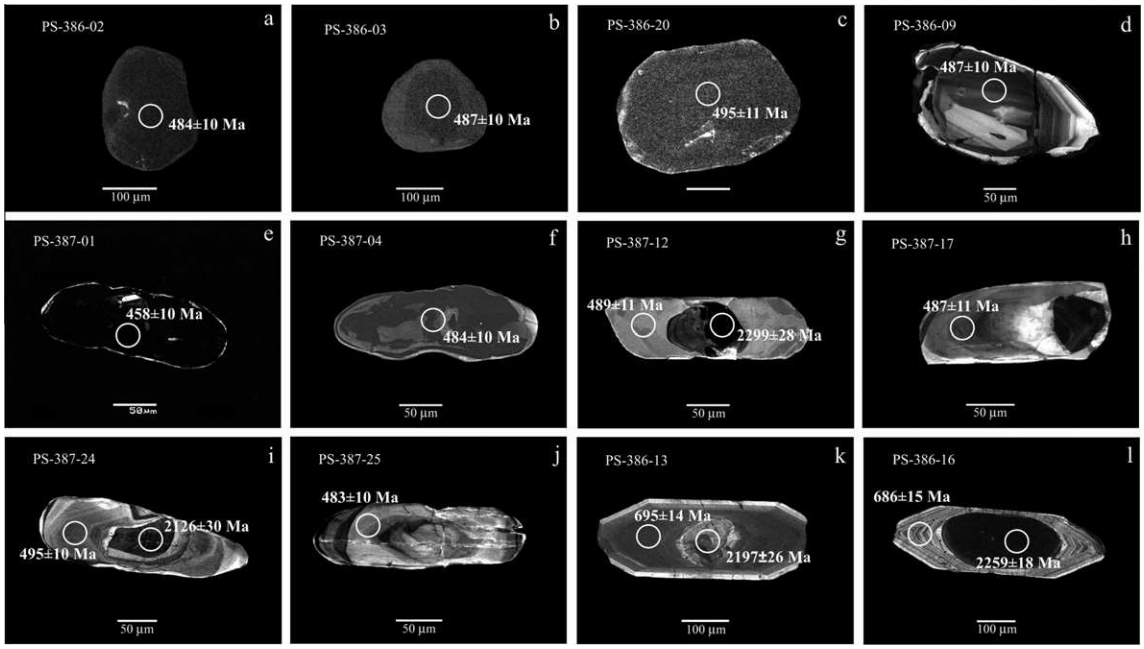

Fig. 6. Cathodoluminescence (CL) images of dated zircons. Circles indicate the positions of LA-ICPMS analytical spots (spot size = 30 μm). The Hf isotopic analyses were performed on the same spots with a slightly wider laser beam (50 μm).

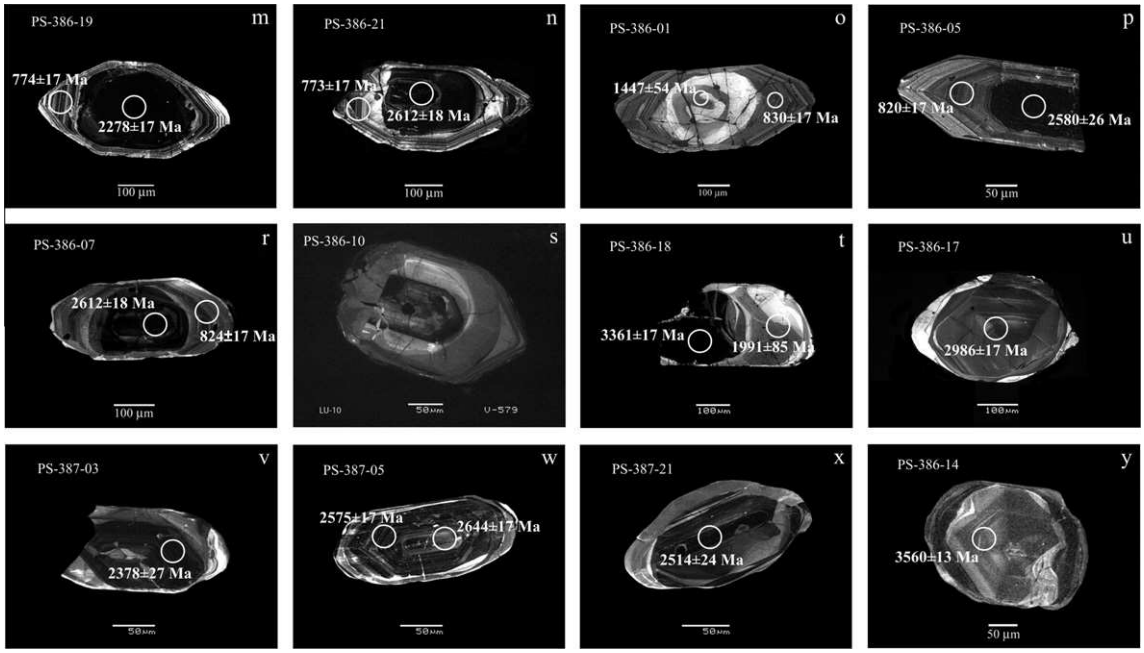

Fig. 6 (*continued*)

concordant zircons (Nos. 16 and 19 in Table 4) have negative $\varepsilon_{Hf}(t)$ of −5.4 to −5.8, corresponding to Hf_{DM} model ages of 3.9–3.4 Ga (t_{Hfc} = 3.5–4.0 Ga).

Paleoproterozoic and Archean zircons and inherited cores from sample PS-386, irrespective of internal structure and morphology, exhibit a continuous range of $\varepsilon_{Hf}(t)$ values from −32.8 to −0.6 and Hf_{DM} model ages of 2.3–3.9 Ga (t_{Hfc} = 2.4–4.0 Ga). Recalculated to apparent discordia ages (see above) they give $\varepsilon_{Hf}(t)$ from −28.7 to +4.0. One inherited core (No. 4 in Table 4) exhibits a mantle-like value of $\varepsilon_{Hf}(t)$ = +7.6.

Zircons and cores with Paleoproterozoic to Neoarchean $^{206}Pb/^{207}Pb$ ages of sample PS-387 have negative $\varepsilon_{Hf}(t)$ values of −6.1 to +5.4 and Neoarchean Hf_{DM} model ages of 2.6–2.8 Ga (t_{Hfc} = 2.7–2.9 Ga) (Table 4). Recalculated to discordia age ca. 2.6 Ga (see above) these zircons yield high positive $\varepsilon_{Hf}(t)$ values of +4.1 to +8.0 that may suggest crystallization from mantle-derived or crust–mantle mixed melts (ε_{Hf} for the upper mantle at 2.6 Ga is +7.8).

5. Discussion

5.1. Approximate age of deposition and provenance of the Slyudyansky metasediments

The youngest zircon ages obtained are 458 ± 10 from sample PS-387 and 487 ± 6 Ma from samples PS-386 and PS-387. Zircons with a mean age of 488 ± 10 Ma from sample PS-386 are subhedral, short-prismatic to isometric with uniform dark-gray luminescence, low Th/U (0.012–0.056) and $^{176}Lu/^{177}Hf$ (0.000036–0.000043) ratios. Such features are typical of metamorphic zircon (Chen et al., 2010) and suggest crystallization during granulite-facies metamorphism. These zircons are characterized by $\varepsilon_{Hf}(t)$ values of −11.1 to −12.3 (weighted average is −11.8 ± 1.6) and Mesoproterozoic Hf model ages $t_{Hf(DM)}$ of 1.5–1.6 Ga that are younger than whole-rock model Nd ages of 2.1–2.2 Ga. However, the crustal model ages t_{Hfc} of 1.8–1.9 Ga are closer or identical to the whole-rock Nd model ages.

Zircons with mean ages of 486 ± 8 Ma and 458 ± 10 Ma from sample PS-387 have variable Th/U ratios of 0.034–0.77 and higher ratios of $^{176}Lu/^{177}Hf$ = 0.000256–0.000817 as compared to those from sample PS-386 (Tables 2 and 3). In come cases, as shown in the CL images of Figs. 5g–j, oscillatory zoning is partially preserved. These zircons may be considered to have formed by dissolution–recrystallization with protolith inheritance (Chen et al., 2010). The 486 ± 8 Ma and 458 ± 10 Ma old zircons have different Hf isotopic characteristics with mean $\varepsilon_{Hf}(t)$ values of −42.2 ± 4.5 and −30.6 ± 1.3, and Hf_{DM} model ages of 2.6–2.9 Ga and 2.2–2.3 Ga respectively. These model ages are younger than whole-rock Nd model ages of 2.8–3.0 Ga (t_{Ndc} = 3.3 Ga). The crustal zircon model ages t_{Hfc} correspond to 3.5–3.6 Ga for the 486 Ma zircons and 2.8 for the 458 Ma zircons. Therefore, the Hf model ages of the metamorphic zircons, even with relicts of magmatic zoning and high Th/U ratios, may be used to identify of crust-forming events and provenance, but with great caution. However, we will not use these zircon Hf model ages in following discussion.

The mean zircon age of 487 ± 6 Ma is in good agreement with single zircon ages for two syn-metamorphic trondhjemites at 488 ± 1 and 488.0 ± 0.5 Ma and a concordant zircon age of 478 ± 2 Ma for an enderbite (Kotov et al., 1997; Salnikova et al., 1998). The age of ca. 480 Ma was considered to correspond to the peak of the granulite-facies metamorphism in the Slyudyansky Complex (Kotov et al., 1997). On the other hand, the age of 458 ± 10 is in good agreement with the age of a post-metamorphic amphibole-two-pyroxene quartz syenite (471 ± 2 Ma; Kotov et al., 1997; Salnikova et al., 1998) and the age of a porphyry plagioclase–microcline granite (467 ± 3 Ma; Stepanov et al., 2009). In summury, the early Paleozoic ages for detrital zircons from metagraywacke samples of the Slyudyansky Complex obtained in this study correspond to the time of Cambro-Ordovician amphibolite- and granulite-facies metamorphism. We emphasize that they do not reflect the ages and isotopic characteristcs of the sedimentary source(s).

Another group of concordant and near-concordant ages obtained for detrital zircons from biotite–garnet–hyperstene plagiogneiss sample PS-386 are 691 ± 20 Ma, 774 ± 24 Ma and 825 ± 20 Ma. These zircons are of magmatic origin as shown by oscillatory zoning and Th/U of 0.12–0.62. Thus, the depositional age of metagraywacke in the Slyudyansky Complex is not older than 670–710 Ma. The younger age limit is constrained by the ages of 487 ± 6 Ma for metamorphic zircons and 488.0 ± 0.5 Ma for syn-metamorphic trondhjemites (Salnikova et al., 1998). Consequently,

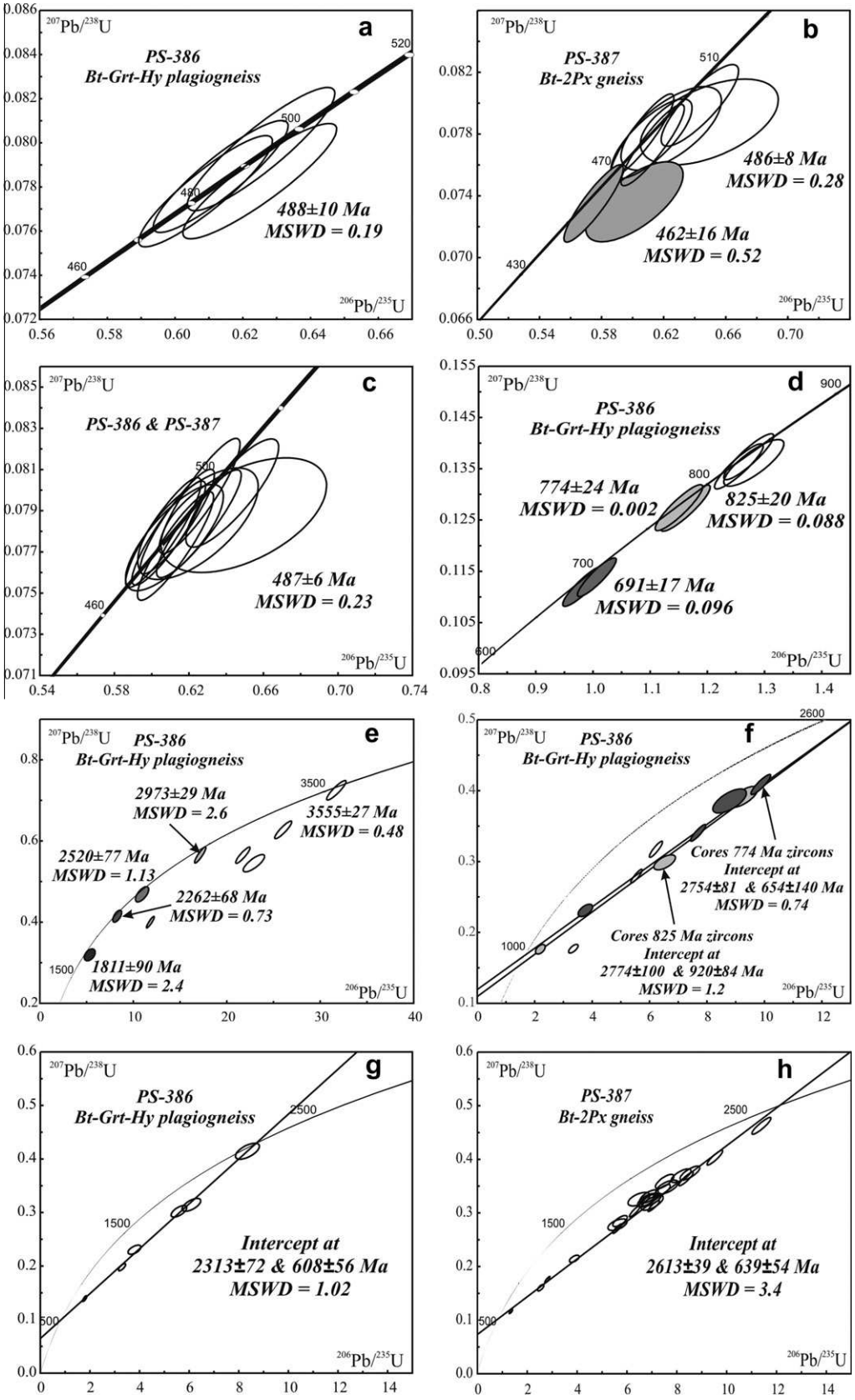

Fig. 7. Concordia diagram showing zircon ages for biotite–garnet–hyperstene-plagioclase gneiss sample PS-386 and biotite-two-pyroxene–plagioclase gneiss sample PS-387 of the Slyudyansky Complex.

deposition of clastic sediments in the Slyudyansky Complex took place in the Neoproterozoic or Cambrian.

The Neoproterozoic zircons exhibit a wide range of negative $\varepsilon_{Hf}(t)$ values from −21.3 to −7.5 and Paleoproterozoic Hf_{DM} model

Table 4
Hf isotopic data for zircons from metasedimentary rocks of the Slyudyansky Complex.

No	No U–Pb	Analysis	Age, Ma	$^{176}Yb/^{177}Hf$	1σ	$^{176}Lu/^{177}Hf$	1σ	$^{176}Hf/^{177}Hf$	1σ	$\varepsilon_{Hf}(t)$	t_{HfDM}, Ma	t_{Hfc}, Ma	Commemts
Biotite–garnet–hyperstene plagiogneiss PS-386													
1	1	PS-386-01-1	1447	0.002454	0.000016	0.000027	0.000001	0.281065	0.000037	−28.4	3.0	3.4	Core NP
2	3	PS-386-02	487	0.003750	0.000034	0.000043	0.000001	0.282128	0.000015	−12.1	1.5	1.9	
3	4	PS-386-03	487	0.003287	0.000050	0.000036	0.000000	0.282157	0.000016	−11.1	1.5	1.8	
4	5	PS-386-04	1939	0.021030	0.000880	0.000334	0.000010	0.281546	0.000018	−0.6	2.3	2.5	Core NP
5	6	PS-386-05-1	2580	0.090337	0.002000	0.001283	0.000025	0.280970	0.000016	−8.1	3.2	3.4	Core NP
6	7	PS-386-05-2	825	0.054370	0.000540	0.000848	0.000003	0.281810	0.000022	−16.3	2.0	2.4	
7	8	PS-386-06-1	1476	0.050064	0.000370	0.000721	0.000005	0.280970	0.000018	−31.8	3.2	3.6	
8	9	PS-386-06-2	2230	0.044707	0.000740	0.000592	0.000006	0.280972	0.000017	−14.8	3.1	3.4	Core NP
9	10	PS-386-07-1	2442	0.071468	0.002600	0.000987	0.000031	0.280808	0.000020	−16.5	3.4	3.7	Core NP
10	11	PS-386-07-2	825	0.040596	0.000560	0.000664	0.000011	0.281734	0.000017	−18.9	2.1	2.5	
11	12	PS-386-07-3	825	0.037500	0.000360	0.000588	0.000004	0.281665	0.000023	−21.3	2.2	2.6	
12	16	PS-386-10-2	2296	0.006012	0.000081	0.000078	0.000002	0.280854	0.000031	−16.7	3.3	3.6	Centre
13	17	PS-386-11	3497	0.011256	0.000230	0.000182	0.000003	0.280408	0.000016	−4.9	3.8	4.0	
14	18	PS-386-12	2559	0.023961	0.000210	0.000333	0.000002	0.280845	0.000022	−11.4	3.3	3.5	
15	19	PS-386-13-1	2197	0.036988	0.000420	0.000567	0.000007	0.280789	0.000025	−22.0	3.4	3.7	Core NP
16	21	PS-386-14	3560	0.060444	0.000250	0.000706	0.000001	0.280382	0.000021	−5.7	3.9	4.0	
17	23	PS-386-15-2	3479	0.049594	0.000650	0.000719	0.000012	0.280520	0.000015	−2.7	3.8	3.8	Core
18	25	PS-386-16-2	691	0.078415	0.001400	0.001111	0.000030	0.282061	0.000022	−10.4	1.7	2.0	
19	26	PS-386-17	2986	0.080232	0.002000	0.000774	0.000008	0.280773	0.000022	−5.1	3.4	3.5	
20	27	PS-386-18-1	1991	0.031551	0.000260	0.000332	0.000002	0.280720	0.000027	−28.7	3.5	3.9	Edge
21	28	PS-386-18-2	3361	0.063482	0.000210	0.000744	0.000006	0.280575	0.000026	−3.5	3.7	3.8	Core
22	31	PS-386-20	487	0.004706	0.000071	0.000043	0.000000	0.282123	0.000019	−12.3	1.6	1.9	
23	34	PS-386-21-3	774	0.069533	0.001500	0.000950	0.000021	0.282046	0.000026	−9.1	1.7	2.0	
24	35	PS-386-22-1	2500	0.013040	0.001600	0.000177	0.000025	0.281132	0.000029	−2.3	2.9	3.0	Core NP
25	36	PS-386-22-2	774	0.089333	0.002000	0.001239	0.000038	0.282029	0.000016	−9.9	1.7	2.0	
Biotite-two-pyroxene gneiss PS-387													
26	37	PS-387-01	458	0.064018	0.001500	0.000817	0.000015	0.281645	0.000023	−30.1	2.2	2.8	
27	39	PS-387-03	2378	0.091975	0.000690	0.001123	0.000009	0.281402	0.000027	3.0	2.6	2.7	
28	43	PS-387-05-2	2644	0.070521	0.001600	0.001171	0.000082	0.281267	0.000039	4.1	2.8	2.8	Centre
29	45	PS-387-07-1	2532	0.041629	0.000540	0.000542	0.000005	0.281272	0.000040	2.8	2.7	2.8	Centre
30	52	PS-387-12-2	487	0.024193	0.000130	0.000255	0.000003	0.281163	0.000039	−46.3	2.9	3.6	Rim
31	56	PS-387-16	458	0.054490	0.001900	0.000637	0.000023	0.281595	0.000034	−31.8	2.3	2.8	
32	57	PS-387-17	487	0.023485	0.000073	0.000353	0.000001	0.281348	0.000035	−39.8	2.6	3.3	
33	61	PS-387-21	2514	0.080032	0.003400	0.001037	0.000025	0.281379	0.000034	5.4	2.6	2.7	
34	64	PS-387-24-1	2126	0.038635	0.000690	0.000683	0.000025	0.281286	0.000040	−6.1	2.7	2.9	Core Pz
35	65	PS-387-24-2	487	0.025675	0.000120	0.000446	0.000003	0.281319	0.000022	−40.9	2.7	3.3	Rim
36	66	PS-387-25	487	0.015740	0.000019	0.000256	0.000002	0.281199	0.000039	−45.0	2.8	3.5	

Notes. No U–Pb – serial number of analysed sample in the Table 3. Age – weighted average $^{206}Pb/^{238}U$ and $^{207}Pb/^{206}Pb$ ages for concordant zircons and individual $^{207}Pb/206Pb$ ages for the discordant zircons. $\varepsilon_{Hf}(t)$ values calculated on the $^{207}Pb/^{206}Pb$ ages of discordant zircons. Core NP – cores of the Neoproterozoic zircons.

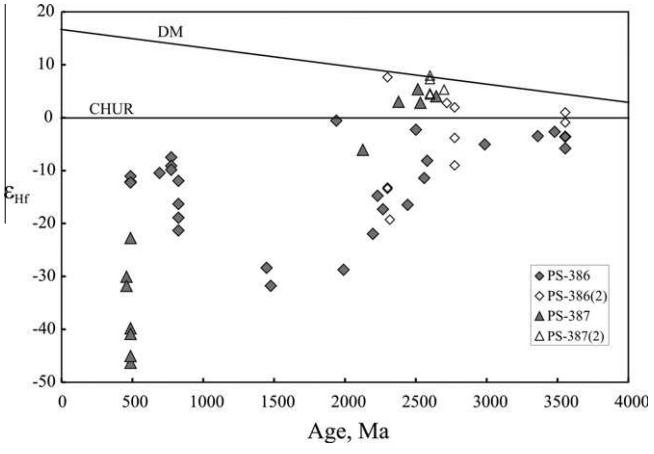

Fig. 8. ε_{Hf} vs. age diagram for zircons from metasedimentary rocks of the Slyudyansky Complex. PS-386(2) and PS-387(2) are isotopic compositions recalculated on an assumed zircon Concordia intercept age (see text for explanation).

ages of 1.7–2.2 Ga. Zircon Hf "crustal" model ages t_{Hfc} vary fairly in the range of 2.0–2.6 Ga. Thus, the Neoproterozoic zircons crystallized from melts derived from Neoarchean to Paleoproterozoic sources. At the same time these zircons contain inherited cores that probably crystallized at ca. 2.7–2.8 and ca. 2.2–2.3 Ga from crustal melts with Hfc model ages of 3.4–3.9 and 2.5 Ga. Such characteristics may be explained by interaction of juvenile Neoproterozoic melts with Archean and Paleoproterozoic crust. Note that another group of inherited cores in the Neoproterozoic zircons have low Th/U ratios from 0.080 to 0.076 and minimum $^{207}Pb/^{206}Pb$ ages of 2278–2259 Ma. These are likely remnants of metamorphic zircons that crystallized during granulite-facies metamorphism. Thus, the source(s) of clastic metasediments in the Slyudyansky Complex is/are ca. 3.9–2.5 Ga Archean to Palaeoproterozoic continental crust mixed with 0.82–0.69 Ga juvenile Neoproterozoic material.

The presence of Paleoproterozoic rocks in the provenance area(s) of the Slyudyansky metasediments is also indicated by near-concordant zircons with ages of 1991 ± 85 and 2296 ± 30 Ma as well as zircons with thin zircon metamorphic rims and ages of 1957–2230 Ma. These zircons are characterized by negative $\varepsilon_{Hf}(t)$ values of −16.7 to −28.7 and Archean Hfc model ages of 3.6–3.9 Ga.

Other detrital zircons and cores from biotite–garnet–hypersten-e plagiogneiss sample No PS-386 show a wide range of Archean ages (2520 ± 77, 2973 ± 29 and 3555 ± 27 Ma) reflecting the source(s) of the original sediment. Hf isotopic analysis of these zircons suggests a long-lived crustal source and t_{Hfc} = 3.0–4.0 Ga.

In contrast, the discordant zircons from biotite-two-pyroxene plagiogneiss sample PS-387 have positive $\varepsilon_{Hf}(t)$ values of +5.4 to +3.0, crustal model ages t_{Hfc} of 2.7–2.8 Ga, and $^{207}Pb/^{206}Pb$ ages of 2644–2378 Ma. $\varepsilon_{Hf}(t)$ values, when recalculated to a discordia age of 2.6 Ga, vary from +4.1 to +8.0, and are close to the value

for the depleted mantle at that time (Fig. 8). These data point to a short-lived ca. 2.6 Ga juvenile source for the Slyudyansky metasediments. However, the Nd whole-rock model ages of 2.8–3.0 Ga also suggest the presence of older crust in the source area(s).

Nd model ages for other samples of the Slyudyansky metasediments ($t_{Nd(DM)}$ = 1.7–2.2 Ga, t_{Ndc} = 1.9–2.2 Ga) are in good agreement with zircon Hf model ages for the Neoproterozoic zircons ($t_{Hf(DM)}$ = 1–7–2.2 Ga, t_{Hfc} = 2.0–2.6 Ga). The whole-rock Nd isotopic data suggest that Neoproterozoic rocks were the main source for the Slyudyansky metasediments, whereas Paleoproterozoic and Archean rocks only played a subordinate role. Rocks with Nd model ages younger 2 Ga are rare in the Siberian craton (Jahn et al., 1988; Kovach et al., 1999, 2000; Kotov, 2003; Rosen and Turkina, 2007) and are assumed, at least partially, to reflect a non-Siberian provenance.

The detrital zircon record and the above discussion indicate that the metasediments in the Slyudyansky Complex were deposited in the time range Neoproterozoic to Cambrian, between ca. 0.69 and 0.49 Ga. Their heterogeneous source(s) consisted of both long-lived Archean (ca. 3.6–2.5 Ga) and Paleoproterozoic (ca. 2.3–2.0 Ga) ($\varepsilon_{Hf}(t)$ = −13.2 to −28.7, t_{Hfc} = 2.5–4.0 Ga) as well as juvenile ($\varepsilon_{Hf}(t)$ = +4.1 to +8.9, t_{Hfc} = 2.7–2.8 Ga) crust mixed with juvenile material during 0.82–0.69 Ga magmatism.

Ages for detrital zircons of 0.90–0.70, 1.52, 1.94 and 2.56 Ga were obtained from high-grade metasedimentary rocks of the Moren and Erzin Complexes in the Western Sangilen terrane of the Tuva–Mongolian microcontinent (Fig. 2) (Kozakov et al., 2005), and these metasediments were intruded by granitoids at 536 ± 6 Ma (Kozakov et al., 1999; Salnikova et al., 2001). Neoproterozoic detrital zircons were also found in metasediments of the Khoboi (ca. 1.06–0.62 Ga) and Orso (ca. 0.86–0.75 Ga) granulite-facies complexes of the Olkhon metamorphic terrane farther northeast (Gladkochub et al., 2010). Thus, we conclude that the clastic sedimentary sequences occurring in early Paleozoic (Cambro-Ordovician) high-grade complexes in the eastern CAOB were probably deposited in late Neoproterozoic (Cryogenian–Ediacaran) time.

5.2. Implications for crustal growth in the CAOB

Many geodynamic models emphasize a significant role of Precambrian microcontinents and individual arc terranes in the formation and evolution of the CAOB (e.g., Zonenshain et al., 1990; Mossakovsky et al., 1993; Berzin et al., 1994; Badarch et al., 2002; Parfenov et al., 2004; Kröner et al., 2007; Windley et al., 2007; Rojas-Agramonte et al., 2011). These are in contrast to the evolutionary model of a single, long-lived island arc (Sengör et al., 1993). A particularly characteristic feature of the CAOB is the wide distribution of granitoids with juvenile Nd isotopic compositions (Kovalenko et al., 1996, 2004; Jahn et al., 2000, 2004). The ages and isotopic data obtained in this study provide important constraints on the time of deposition and provenance of metasedimentary rocks of early Paleozoic high-grade complexes in southern Siberia and also constrain crustal growth models for the CAOB.

The Neoproterozoic ages of detrital zircons discussed above coincide with the assumed time of rifting at ca. 825–740 Ma that led to the break-up of the Rodinia supercontinent and opening of the Paleo-Asian Ocean at ca. 750–630 Ma (Yarmolyuk et al., 2005b, 2006; Li et al., 2008). Our ages are also compatible with derivation of the sediments from blocks rifted off or forming around Rodinia. Consequently, in order to evaluate possible source regions for late Neoproterozoic to Cambrian clastic sediments that now occur in early Paleozoic high-grade complexes in southern Siberia, it is necessary to discuss the Precambrian geochronology of the eastern CAOB and surrounding cratons (Siberia, Tarim, North China and South China).

Paleomagnetic and geological reconstructions regarding the position of the Siberian craton within Rodinia are highly controversial (Khudoley et al., 2001; Yarmolyuk and Kovalenko, 2001; Yarmolyuk et al., 2005b, 2006; Li et al., 2008; Pisarevsky et al., 2008; Metelkin et al., 2007; Levashova et al., 2010; Kheraskova et al., 2010). One school of thought assumed that the southern margin (in present-day coordinates) of the Siberian craton was facing the northern Laurentian–South China cratons at ca. 1100–780 Ma with a common shelf or unknown blocks between them (Khudoley et al., 2001; Pisarevsky et al., 2008; Yarmolyuk and Kovalenko, 2001; Yarmolyuk et al., 2005b; Li et al., 2008; Metelkin et al., 2007). The other school suggested that Siberia and Laurentia were connected via their northern margins (Vernikovsky et al., 2003) or that Siberia and the North China–Tarim cratons were not part of Rodinia but were surrounded by open oceans (Khain et al., 2003; Kheraskova et al., 2010; Rojas-Agramonte et al., 2011). Despite these differences, all authors assume derivation of the CAOB microcontinents from some of surrounding cratons.

The sources of Archean and Paleoproterozoic zircons in the Neoproterozoic to early Paleozoic metasediments reported here are difficult to specify because detrital ages of ca. 3.6, 2.8–2.7, 2.3–2.2 and 2.0 Ga are common in many Precambrian cratons. Magmatic and metamorphic events at ca. 3.4–3.2, 2.8, 2.66 and 1.86–1.85 Ga and detrital zircons with ages of ca. ⩾2.7, 2.3 and 2.0–1.95 Ga are widespread in the Sharyzhagai terrane (Fig. 1) of the southwestern Siberian craton (Turkina et al., 2007, 2009, 2010; Poller et al., 2005; Bibikova et al., 2006; Salnikova et al., 2007). Crust-forming events at ca. 3.8–3.5, 3.3–3.2, 3.0–2.9 and 2.2–2.0 Ga are typical for the Aldan Shield (Jahn et al., 1998; Kotov, 2003). Moreover, the intrusive events of 2.76–2.73, 2.52–2.40, 2.07 and 1.97–1.87, 1.70–1.74 Ga post-collisional and anorogenic granitoids are also well recognized in the Aldan Shield (Kotov, 2003). Magmatic and metamorphic events at ~2.85–2.83 and 2.65–2.60 Ga occurred in the Stanovoy fold belt (Glebovitsky et al., 2009). Note, however, that ca. 2.9–2.7 and 2.6–2.5 Ga crust-forming events are not characteristic of the Aldan Shield (Nutman et al., 1992; Neymark et al., 1993; Kotov et al., 1995; Salnikova et al., 1996; Jahn et al., 1998; Kotov, 2003) and the Siberian craton as a whole (Kovach et al., 2000; Rosen and Turkina, 2007).

A zircon xenocryst at 3.6 Ga and magmatic events at ca. 2.8, 2.7–2.6, 2.55–2.35 and 2.0–1.8 Ga are characteristc of the Tarim craton (Lu et al., 2008; Shu et al., in press). 2.67 Ga old trondhjemites are juvenile with t_{NdDM} = 2.7 Ga (Lu and Yuan, 2003), whereas much of the Tarim crust was formed in the period 2.1–1.7 Ga (Hu et al., 2000). The basement of the Yangtze craton mainly consists of Paleoproterozoic (2.0–1.8 Ga) magmatic and metamorphic rocks with only sporadic occurrences of Archean rocks with ages of ca. 3.3–2.7 Ga and rare granitoid intrusions at ca. 2.5–2.4 Ga (Chen and Jahn, 1998; Qiu et al., 2000; Zhang et al., 2006). Archean (ca. 3.57–2.66 Ga) and Paleoproterozoic (ca. 2.38–2.14 Ga and 1.95–1.73 Ga) detrital zircons were identified in the 1675 ± 8 Ma Dahongshan Group (Greentree and Li, 2008) and in the ca. 1.0–0.96 Ga Kunyang Group (Greentree et al., 2006). Magmatic and metamorphic activity at ca. 2.9–2.7, 2.6–2.45, 2.36–2.0 and 1.95–1.75 Ga with a major crust-forming event at ca. 2.5 Ga are typical of the North China craton (Zhai et al., 2005; Zhao et al., 2005; Wu et al., 2005; Wan et al., 2010). Detrital zircon age peaks at 2.8–2.6, 2.4–2.35 and 2.1–1.85 Ga were established by Darby and Gehrels (2006) for Neoproterozoic to Ordovician sediments from the Ordos Block in the western part of this craton.

On the other hand, events at ca. 2.83–2.73, 2.65 and 2.4–2.3 Ga were identified in the Baidrag Block of the Dzabkhan microcontinent and the Gargan Block of the Tuva–Mongolian microcontinent within the CAOB (Fig. 2) (Early Precambrian..., 1993; Kozakov et al., 1997, 2007c; Kovach et al., 2004; Anisimova et al., 2009). An intrusive age of 2219 ± 25 Ma was also determined for

granite-gneisses in the Tarbagatai Block of the Dzabkhan microcontinent (Kozakov et al., 2009a). All these events seem to be comparable to those identified in the Tarim, North China and South China cratons. Thus, microcontinental blocks of the CAOB derived from these cratons may be sources of ca. 2.8–2.6 Ga and 2.3–2.2 Ga zircons in Neoproterozoic metasediments of the early Paleozoic high-grade complexes.

Recent investigations show growing evidence for widespread magmatism in the early Neoproterozoic ca. 1.0–0.72 Ma (early Baikalian in the Russian literature) in different parts of the eastern CAOB. This magmatism is represented by oceanic and island arc complexes such as the Dunzhugur (~1020 Ma, Khain et al., 2002) and Shishkhid (800 ± 3 Ma, Kuzmichev et al., 2005) ophiolites, the Oka accretionary prism (⩾753 ± 16 Ma, Kuzmichev et al., 2007) in the Tuva–Mongolian microcontinent, the Nyurundukan and Shaman metabasalts of the Baikal-Muya belt (ca. 1.0–0.9 Ga, Rytsk et al., 2001; 939 ± 11 to 892 ± 16 Ma, Gordienko et al., 2009), and the Songino ophiolite complex in northern Mongolia (>0.81 < 1.2 Ga, Yarmolyuk et al., 2009). Neoproterozoic tectonothermal events are also documented in continental margin arcs and reworked metamorphic basement (e.g., the Sarkhoy formation of the Tuva–Mongolian microcontinent (778 ± 7 Ma, Kuzmichev and Larionov, 2011), the Anamakit-Muya zone of the Baikal-Muya Belt (825 ± 3 to 723 ± 4 Ma, Rytsk et al., 2007, 2009 and references therein), the Songino block of the northen Mongolia (810–790 Ma, Kozakov et al., 2009b), and the Baga Bogd block (983 ± 6 to 954 ± 8 Ma, Demoux et al., 2009a,b) and Totoshan-Ulanul block of the South Gobi microcontinent (952 ± 8 Ma and 919 ± 16 Ma; Yarmolyuk et al., 2005a,b; Wang et al., 2001). Bimodal volcanic rocks of the Dzabkhan Formation (804 ± 8 to 773 ± 4 Ma; Levashova et al., 2010) and alkaline granitoids (755 ± 3 Ma; Yarmolyuk et al., 2008) of rift origin occur in the Dzabkan microcontinent. The age patterns of detrital and xenocrystic zircons of Neoproterozoic and Paleozoic arcs and microcontinental terranes in Mongolia show the dominance of two age ranges at ca. 0.6–0.35 and 1.24–0.70 Ga, with peaks at 815, 890 and 1018 Ma as well as minor peaks between ca. 1240 and 2570 Ma Rojas-Agramonte et al. (2011).

Neoproterozoic rift-related magmatism in the Siberian craton (Fig. 1) occurred in the Olokit zone of the Baikal-Patom fold belt (Fig. 1) (727 ± 18 to 711 ± 6 Ma subvolcanic K-rhyolites, Rytsk et al., 2002; 707 ± 40 Ma gabbro-diabase, gabbro-norite sills and dikes, 673 ± 22 dunite–troctolite–gabbro massifs, Amelin et al., 1996), in the East Angara fold bet (780 ± 4 Ma and 753 ± 6 Ma bimodal Rybinskaya and Verkhnevorogovskaya formations; Nozhkin et al., 2008, 2009) and along the southern and southwestern craton margins (ca. 780–740 Ma mafic dike swarms of the Biryusa and Sharyzhalgay uplifts (Gladkochub et al., 2006) as well as 654 ± 7 to 632 ± 2 Ma alkalic–ultrabasic complexes with carbonatites (Yarmolyuk et al., 2005a).

Such Neoproterozoic ages are also typical for the Tarim craton (see review by Rojas-Agramonte et al. (2011) and Long et al. (2011)). Lu et al. (2008) and Shu et al. (in press) suggested that the Tarimian orogeny (ca. 1.06–0.90 Ga) was related to the assembly of Rodinia. Subsequent rifting and/or plume-related magmatism (granite, bimodal volcanism, mafic dike swarms) between ca. 0.82 Ga and 0.70 Ga were possibly associated with break-up of the supercontinent (Rojas-Agramonte et al., 2011). The Yangtze and Cathasia blocks of southern China collided at ca. 1.14–0.90 Ga (Greentree et al., 2006; Li et al., 2005). Neoproterozoic magmatism in southern China defines four major peaks at ca. 825 Ma, 800 Ma, 780 Ma and 750 Ma (Li et al., 2005). This magmatism is thought by some authors to be plume-induced and was coeval with continental rifting and the assumed break-up of Rodinia (Li et al., 2008). In contrast, Grenville-age and early Neoproterozoic magmatic or metamorphic events are not known from the North China craton (Rojas-Agramonte et al., 2011).

From the above, a geodynamic model for deposition of Neoproterozoic to Cambrian sediments in the eastern CAOB can be proposed. During the period 1300–900 Ma, the growth of oceanic crust was compensated by subduction zones around the margins of Rodinia. During the same period, ca. 1020–780 Ma ophiolites and island arc complexes were formed. These magmatic rocks are represented by the Dunzhugur (Khain et al., 2002), Nyurundukan (Rytsk et al., 2001), Shishkhid (Kuzmichev et al., 2005), Sarkhoy (Kuzmichev and Larionov, 2011) and Songino (Yarmolyuk et al., 2009) complexes in Siberia and Mongolia and the Sibao arc volcanic rocks along the northern margin of the Yangtze craton (Ling et al., 2003). The ophiolites and island arcs were accreted to the cratons and were metamorphosed at ca. 0.82–0.78 Ga (Rytsk et al., 2007; Kozakov et al., 2009b). Maruyama et al. (2007) and Li et al. (2008) inferred a superplume and continental rifting between ca. 825–740 Ma in the South China craton. At this time, the continental crust was reworked along the margins of the cratons of Rodinia. After break-up of the supercontinent and opening of the Paleo-Asian Ocean at ca. 750–630 Ma (Yarmolyuk and Kovalenko, 2001; Yarmolyuk et al., 2005b, 2006; Li et al., 2008), the composite basement blocks (juvenile and reworked during formation of Neoproterozoic crust) were rifted off Rodinia. These blocks drifted from the Tarim and South China cratons and from northeastern Gondwana into the Paleo-Asian Ocean and eventually collided with late Neoproterozoic (0.70–0.62 Ga) oceanic plateaux and volcanic arcs that formed in this ocean (Kovach et al., 2005; Rytsk et al., 2007; Terent'eva et al., 2008). Paleomagnetic (Kravchinsky et al., 2010) and geochronological (Rytsk et al., 2007) data suggest that amalgamation of Eastern Sayan, Tuva, the central part of the Mongolian terranes and possibly the Barguzin superterrane, and formation of the Tuva–Mongolian microcontinet and Barguzin superterranes occurred before the Ediacaran–Early Cambrian. The Siberian craton was situated in an open ocean, whereas the Tuva–Mongolian microcontinent and Barguzin superterranes were in close proximity to the Siberian craton with some space between them at ca. 560–520 Ma (Kravchinsky et al., 2010). Sediments derived from these composite terranes and volcanic arcs were deposited in ensialic bark-arc or fore-arc settings. These sediments have whole-rock Nd compositions intermediate between Archean and Neoproterozoic crustal sources. The detrital zircons have ages ranging from Archean–Paleoproterozoic to the Neoproterozoic (0.90–0.62 Ga) and show crustal Hf signatures as seen in metasediments of the Slyudyansky Complex.

Extensive processes of plate convergence and formation of oceanic islands and island arcs occurred in the Paleo-Asian Ocean at ca. 600–545 Ma (Pfänder et al., 2002; Gibsher et al., 2001; Buslov et al., 2002; Kozakov et al., 2002; Kovalenko et al., 2004; Gordienko et al., 2006; Safonova et al., 2008; Utsunomiya et al., 2009; Yarmolyuk et al., 2011; Kovach et al., 2011). Finally, accretion of latest Neoproterozoic–early Cambrian oceanic and island arc complexes together with composite microcontinents and their deformation and metamorphism at 510–480 Ma (Kotov et al., 1997; Kozakov et al., 1999, 2001; Salnikova et al., 1998, 2001; Donskaya et al., 2000; Gladkochub et al., 2010; Rytsk et al., 2009) resulted in the formation of early Paleozoic high-grade metamorphic complexes.

6. Conclusion

Our zircon ages, Hf isotopic data, and whole-rock Nd isotopic compositions provide a strong constraints to the timing of deposition and provenance of metasedimentary rocks from the early Paleozoic high-grade Slyudyansky Complex in southwestern Siberia. The data also constrain models of crustal growth in the CAOB.

1. Detrital zircon ages of 0.90–0.62 Ga for clastic metasediments that occur in an early Paleozoic high-grade complex indicate that deposition occurred in the Neoproterozoic to earliest Paleozoic, between ca. 0.69–0.62 and 0.54–0.49 Ga.
2. Hf isotopic data of 0.82–0.69 Ga detrital zircons indicate that the sources comprise Archean and Paleoproterozoic rocks (t_{Hfc} = 2.5–3.9 Ga), that were mixed with juvenile 0.82–0.69 Ga material durinmg Neoproterozoic magmatism.
3. An additional protolith yielded zircon ages of 2.6–2.7 Ga with high positive $\varepsilon_{Hf}(t)$ values of +4.1 to +8.0, and Hf model ages $t_{Hf(DM)} = t_{Hfc}$ = 2.8–2.6 Ga, which is nearly identical to the zircon crystallization ages. These isotopic characteristics suggest that the protolith was juvenile.
4. The whole-rock Nd isotopic data imply that at least part of the Slyudyansky metasediments was derived from a non-Siberian provenance.
5. Crustal development in the eastern CAOB was characterized by reworking of early Precambrian continental crust in the early Neoproterozoic and mixing with late Neoproterozoic–early Paleozoic juvenile material. The tectonic scenario and geodynamic setting for the eastern CAOB in late Neoproterozoic–early Paleozoic were similar to those in the present southwestern Pacific (SW Pacific (Hall, 2009; Metcalfe, 2011).

Acknowledgments

The authors thank A. Kröner and Y. Rojas-Agramonte for providing a manuscript reviewing the geochronology and new detrital zircon ages for the CAOB and surrounding cratons. We benefitted from discussions with I.K. Kozakov, V.V. Yarmolyuk. Work in the Nd isotope laboratory was assisted by N.Yu. Zagornaya. Figs. 1–3 were drawn by G.P. Pleskach. A.N. Komarov prepared perfect zircon mounts. We grateful to A. Kröner and anonymous reviewer for suggesting improvements to the manuscript. This research was jointly supported by the Russian Foundation for Basic Research (RFBR; Grant Nos. 07-05-92001 and 96WIA0100026) and the National Science Council (NSC) of Taiwan (Grant No. 99-2811-M-001-031).

References

Afonin, V.P., Finkelstein, A.L., Borkhodoev, V.J., Gunicheva, T.N., 1992. X-ray fluorescence analysis of rocks by the fundamental parameter methods. X-ray Spectrometry 21, 69–75.

Amelin, Yu.V., Neymark, L.A., Ritsk, E.Yu., Nemchin, A.A., 1996. Enriched Nd-Sr-Pb isotopic signatures in the Dovyren layered intrusion (eastern Siberia, Russia): evidence for source contamination by ancient upper-crustal material. Chemical Geology 129, 39–69.

Amelin, Y., Lee, D.-C., Halliday, A.N., Pidgeon, R.T., 1999. Nature of the Earth's earliest crust from hafnium isotopes in single detrital zircons. Nature 399, 252–255.

Anderson, T., 2002. Correction of common lead in U–Pb analyses that do not report 204Pb. Chemical Geology 192, 59–79.

Anisimova, I.V., Levitsky, I.V., Salnikova, E.B., Kotov, A.B., Levitsky, V.I., Reznitskii, L.Z., Efremov, S.V., Velikoslavinsky, S.D., Barash, I.G., Fedoseenko, A.M., 2009. Age of the Gagran block basement (Eastern Sayan): results of U–Pb geochronological studies. In: IV Russian Conference on Isotope Geochronology, St.-Petersburg, Conference Abstracts 1, pp. 34–35 (in Russian).

Atlas of Geological Maps of Central Asia and Adjacent Areas, 2007. Scale 1:2500000. Tingdong, L., Daukeev, S.Z., Kim, B.C., Tomurtogoo, O., Petrov, O.V., (Eds.-Inchief). Geological Publishing House, Beijing.

Badarch, G., Cunningham, W.D., Windley, B.F., 2002. A new terrane subdivision for Mongolia: implications for the Phanerozoic crustal growth of Central Asia. Journal of Asian Earth Sciences 21, 87–110.

Barash, I.G., Sal'nikova, E.B., Reznitskii, L.Z., Kotov, A.B., Kovach, V.P., Yakovleva, S.Z., Fedoseenko, A.M., 2006. Age relations between metamorphism of the Slyudyanka granulite and the Khamar Daban zoned metamorphic complexes: evidence from U–Pb geochronological data. Doklady Earth Sciences 409A, 905–908.

Belichenko, V.G., Boos, R.G., 1988. The Bokson–Khubsugul–Dzabkhan microcontinent in Paleozoic structure of Central Asia. Russian Geology and Geophysics 12, 20–28.

Belichenko, V.G., Sklyarov, E.V., Dobretsov, N.L., Tomurtogoo, O., 1994. Geodynamic map of the Paleo-Asian ocean. Russian Geology and Geophysics 7-8, 29–41.

Berzin, N.A., Coleman, R.G., Dobretsov, N.L., Zonenshain, L.P., Xuchan, S., Chang, E.Z., 1994. Geodynamic map of Paleo-Asian ocean: eastern segment. Russian Geology and Geophysics 35, 8–28.

Bibikova, E.V., Turkina, O.M., Kirnozova, T.I., Fugzan, M.M., 2006. Ancient plagiogneisses of the onot block of the Sharyzhalgay metamorphic Massif: isotopic geochronology. Geochemica International 3 (3), 310–316.

Black, L.P., Gulson, B.L., 1978. The age of the Mud Tank carbonatite, Strangways Range, Northern Territory. BMR Journal of Australian Geology & Geophysics 3, 227–232.

Black, L.P., Jagodzinski, E.A., 2003. Importance of establishing sources of uncertainty for the derivation of reliable SHRIMP ages. Australian Journal of Earth Sciences 50, 503–512.

Blichert-Toft, J., Albarède, F., 1997. The Lu–Hf isotope geochemistry of chondrites and the evolution of the mantle–crust system. Earth and Planetary Science Letters 148, 243–258.

Buslov, M.M., Watanabe, T., Saphonova, I.Yu., Iwata, K., Travin, A., Akiyama, M.A., 2002. Vendian–Cambrian island arc system of the Siberian continent in Gorny Altai (Russia, Central Asia). Gondwana Research 5, 781–800.

Chen, J., Jahn, B.-M., 1998. Crustal evolution of southeastern China: Nd and Sr isotopic evidence. Tectonophysics 284, 101–133.

Chen, R.-X., Zheng, Y.-F., Liewen Xie, L., 2010. Metamorphic growth and recrystallization of zircon: distinction by simultaneous in situ analyses of trace elements, U–Th–Pb and Lu–Hf isotopes in zircons from eclogite-facies rocks in the Sulu orogen. Lithos 114, 132–154.

Chiu, H.-Y., Chung, S.-L., Wu, F.-Y., Liu, D., Liang, Y.-H., Lin, I-J., Iizuka, Y., Xie, L.-W., Wang, Y., Mei-Fei Chu, M.-F., 2009. Zircon U–Pb and Hf isotopic constraints from eastern Transhimalayan batholiths on the precollisional magmatic and tectonic evolution in southern Tibet. Tectonophysics 477 (1–2), 3–19.

Darby, B.J., Gehrels, G., 2006. Detrital zircon reference for the North China block. Journal of Asian Earth Sciences 26, 637–648.

De Biévre, P., Taylor, P.D.P., 1993. Table of the isotopic compositions of the elements. International Journal of Mass Spectrometry and Ion Processes 123, 149–166.

Demoux, A., Kröner, A., Badarch, GT., Jian, P., Tomurhuu, D., Wingate, M.T.D., 2009a. Zircon ages from the Baydrag Block and the Bayankhongor ophiolite zone: time constraints on late Neoproterozoic to Cambrian subduction- and accretion-related magmatism in Central Mongolia. Journal of Geology 117, 377–397.

Demoux, A., Kröner, A., Liu, D., Badarch, G., 2009b. Precambrian crystalline basement in southern Mongolia as revealed by SHRIMP zircon dating. International Journal of Earth Sciences 98, 1365–1380.

Demoux, A., Kröner, A., Hegner, E., Badarch, G., 2009c. Devonian arc-related magmatism in the Tseel terrane of SW Mongolia: chronological and geochemical evidence. Journal of the Geological Society of London 166, 459–471.

Dergunov, A.B., Kovalenko, V.I., Ruzhentsev, S.V., Yarmolyuk, V.V., 2001. Tectonics, Magmatism, and Metallogeny of Mongolia. Taylor and Francis Group, London–New York, 288pp..

Didenko, A.N., Mossakovskii, A.A., Pecherskii, D.M., Ruzhentsev, S.V., Samygin, S.G., Kheraskova, T.N., 1994. Geodynamics of Paleozoic oceans in Central Asia. Russian Geology and Geophysics 35, 59–75 (in Russian).

Dobretsov, N.L., Buslov, M.M., 2007. Late Cambrian–Ordovician tectonics and geodynamics of Central Asia. Russian Geology and Geophysics 48, 1–12.

Donskaya, T.V., Sklyarov, E.V., Gladkochub, D.P., Mazukabzov, A.M., Salnikova, E.B., Kovach, V.P., Yakovleva, S.Z., Berezhnaya, N.G., 2000. The Baikal collisional metamorphic belt. Doklady Earth Sciences 374 (7), 1075–1079.

Early Precambrian in the Central Asian Fold Belt, 1993. Kozakov, I.K., (Ed.), St. Petersburg, Nauka, 266pp. (in Russian).

Eggins, S.M., Kinsley, L.P.J., Shelley, J.M.G., 1998. Deposition and element fractionation processes during atmospheric pressure laser sampling for analysis by ICP-MS. Applied Surface Science 127–129, 278–286.

Fujimaki, H., 1986. Partition coefficients of Hf, Zr, and REE between zircon, apatite, and liquid. Contribution to Mineralogy and Petrology 94, 42–45.

Gibsher, A.S., Khain, E.V., Kotov, A.B., Salnikova, E.B., Kozakov, I.K., Kovach, V.P., Yakovleva, S.Z., Fedoseenko, A.M., 2001. Late Vendian age of the Khan-Taishiri ophiolite complex of the Western Mongolia. Russian Geology and Geophysics 42, 1179–1185.

Gladkochub, D.P., Wingate, M.T.D., Pisarevsky, S.A., Donskaya, T.V., Mazukabzov, A.M., Ponomarchuk, V.A., Stanevich, A.M., 2006. Mafic intrusions in southwestern Siberia and implications for a Neoproterozoic connection with Laurentia. Precambrian Research, 260–278.

Gladkochub, D.P., Donskaya, T.V., Fedorovskii, V.S., Mazukabzov, A.M., Larionov, A.N., Sergeev, S.A., 2010. The Olkhon metamorphic terrane in the Baikal region: an Early Paleozoic collage of Neoproterozoic active margin fragments. Russian Geology and Geophysics 51, 429–442.

Glebovitsky, V.A., Kotov, A.B., Sal'nikova, E.B., Larin, A.M., Velikoslavinsky, S.D., 2009. Granulite complexes of the Dzhugdzhur–Stanovoi fold region and the Peristanovoi belt: age, formation conditions, and geodynamic settings of metamorphism. Geotectonics 43 (4), 81–91.

Goldstein, S.J., Jacobsen, S.B., 1988. Nd and Sr isotopic systematics of rivers water suspended material: implications for crustal evolution. Earth and Planetary Science Letters 87, 249–265.

Gordienko, I.V., Kovach, V.P., Gorokhovsky, D.V., Sal'nikova, E.B., Kotov, A.B., Yakovleva, S.Z., Zagornaya, N.Yu., Fedoseenko, A.M., Plotkina, Yu.V., 2006. Composition, U–Pb age, and geodynamic setting of island-arc gabbroids and

granitoids of the Dzhida zone (southwestern Transbaikalia, northern Mongolia). Russian Geology and Geophysics 47, 956–962.
Gordienko, I-V., Bulgatov, A.N., Lastochkin, N.I., Sitnikova, V.S., 2009. Composition and U–Pb isotopic age determinations (SHRIMP II) of the ophiolitic assemblage from the Shaman paleospreading zone and the conditions of its formation (North Transbaikalia). Doklady Earth Sciences 429A, 1420–1425.
Greentree, M.R., Li, Z.-X., 2008. The oldest known rocks in south-western China: SHRIMP U–Pb magmatic crystallisation age and detrital provenance analysis of the Paleoproterozoic Dahongshan Group. Journal of Asian Earth Sciences 33, 289–302.
Greentree, M.R., Li, Z.X., Li, X.H., Wu, H., 2006. Late Mesoproterozoic to earliest Neoproterozoic basin record of the Sibao orogenesis in western South China and relationship to the assembly of Rodinia. Precambrian Research 151, 79–100.
Griffin, W.L., Pearson, N.J., Belousova, E., Jackson, S.E., van Achterberg, E., O'Reilly, S.Y., Shee, S.R., 2000. The Hf isotope composition of cratonic mantle: LAM-MC-ICMPS analysis of zircon megacrysts in kimberlites. Geochimica et Cosmochimica Acta 64, 133–147.
Griffin, W.L., Wang, X., Jackson, S.E., Pearson, N.J., O'Reilly, S.Y., Xu, X., Zhou, X., 2002. Zircon chemistry and magma mixing, SE China: in situ analysis of Hf isotopes, Tonglu and Pingtan igneous complexes. Lithos 61, 237–269.
Griffin, W.L., Pearson, N.J., Belousova, E.A., Saeed, A., 2006. Comment: Hf-isotope heterogeneity in zircon 91500. Chemical Geology 233, 358–363.
Günther, D., Heinrich, C.A., 1999. Enhanced sensitivity in laser ablation–ICP mass spectrometry using helium–argon mixtures as aerosol carrier. Journal of Analytical Atomic Spectrometry 14, 1363–1368.
Hall, R., 2009. The Eurasian SE Asian margin as a modern example of an accretionary orogen. In: Cawood, P.A., Kröner, A. (Eds.), Accretionary Orogens in Space and Time: Geological Society of London, Special Publication 318, 351–372.
Hu, A., Jahn, B., Zhang, G., Chen, Y., Zhang, Q., 2000. Crustal evolution and Phanerozoic crustal growth in northern Xinjiang: Nd isotopic evidence. Part I. Isotopic characterization of basement rocks. Tectonophysics 328, 15–51.
Il'in, A.V., 1971. About Tuva–Mongolian Massif. Materials on regional geology of Africa and foreign Asia. Proceeding NII Zarubezhgeologiya 22, 67–73 (in Russian).
Il'in, A.V., 1982. Geologic Evolution of Southern Siberia and Mongolia in the Late Precambrian–Cambrian. Nauka, Moscow, p. 115 (in Russian).
Jackson, S.E., Pearson, N.J., Griffin, W.L., Belousova, E.A., 2004. The application of laser ablation-inductively coupled plasma–mass spectrometry to in situ U–Pb zircon geochronology. Chemical Geology 211, 47–69.
Jacobsen, S.B., Wasserburg, G.J., 1984. Sm–Nd evolution of chondrites and a chondrites. II. Earth and Planetary Science Letters 67, 137–150.
Jahn, B.-M., Gruau, G., Capdevila, R., Cornichet, J., Nemchin, A., Pidgeon, R., Rudnik, V.A., 1998. Archean crustal evolution of the Aldan Shield, Siberia: geochemical and isotopic constraints. Precambrian Research 91, 333–363.
Jahn, B.-M., Wu, F., Chen, B., 2000. Granitoids of the Central Asian Orogenic Belt and continental growth in the Phanerozoic. Transactions of the Royal Society of Edinburgh: Earth Sciences 91, 181–193.
Jahn, B.-M., Capdevila, R., Liu, D.Y., Vernon, A., Badarch, G., 2004. Sources of Phanerozoic granitoids in the transect Bayanhongor–Ulaan Baatar, Mongolia: geochemical and Nd isotopic evidence, and implications for Phanerozoic crustal growth. Journal of Asian Earth Sciences 23, 629–653.
Keto, L.S., Jacobsen, S.B., 1987. Nd and Sr isotopic variations of Early Paleozoic oceans. Earth and Planetary Science Letters 84, 27–41.
Khain, E.V., Bibikova, E.V., Kröner, A., Zhuravlev, D.Z., Sklyarov, E.V., Fedetova, A.A., Kravchenko-Berezhnoy, I.R., 2002. The most ancient ophiolites of the Central Asian Fold Belt: U–Pb and Pb–Pb zircon ages for the Dunzhugur complex, Eastern Sayan, Siberia, and geodynamic implications. Earth and Planetary Science Letters 199, 311–325.
Khain, E.V., Bibikova, E.V., Salnikova, E.B., Kröner, A., Gibsher, A.S., Didenko, A.N., Degtyarev, K.E., Fedetova, A.A., 2003. The Palaeo-Asian ocean in the Neoproterozoic and early Palaeozoic: new geochronologic data and palaeotectonic reconstructions. Precambrian Research 122, 329–358.
Kheraskova, T.N., Didenko, A.N., Bush, V.A., Volozh, Y.A., 2003. The Vendian-early Paleozoic history of the continental margin of eastern Paleogondwana, Paleoasian Ocean, and Central Asian Foldbelt. Russian Journal of Earth Sciences 5, 165–184.
Kheraskova, T.N., Bush, V.A., Didenko, A.N., Samygin, S.G., 2010. Breakup of Rodinia and early stages of evolution of the Paleoasian Ocean. Geotectonics 44, 3–24.
Khudoley, A.K., Rainbird, R.H., Stern, R.A., Kropachev, A.P., Heaman, L.M., Zanin, A.M., Podkovyrov, V.N., Belova, V.N., Sukhorukov, V.I., 2001. Sedimentary evolution of the Riphean-Vendian basin of southeastern Siberia. Precambrian Research 111, 129–163.
Kotov, A.B., 2003. Boundary Constraints on Geodynamic Model of the Aldan Shield Continental Crust Formation. Doctor of Scienes Thesis, St-Petersburg, 78pp.
Kotov, A.B., Kovach, V.P., Salnikova, E.B., Glebovitsky, V.A., Yakovleva, S.Z., Berezhnaya, N.G., Myskova, T.A., 1995. Continental crust age and evolution in the central Aldan granulite–gneiss terrain: U–Pb and Sm–Nd data on granitoids. Petrology 1, 97–108.
Kotov, A.B., Salnikova, E.B., Reznitskii, L.Z., Vasil'ev, E.P., Kozakov, I.K., Yakovleva, S.Z., Kovach, V.P., Berezhnaya, N.G., 1997. Age of metamorphism of the Slyudyanka crystalline complex, Southern Baikal Area: U–Pb geochronology of granitoids. Petrology 5, 338–349.
Kovach, V.P., Kotov, A.B., Beryozkin, V.I., Salnikova, E.B., Velikoslavinsky, S.D., Smelov, A.P., Zagornaya, N.Yu., 1999. Age limits of high-grade metamorphic supracrustal complexes in the Central Aldan Shield: Sm–Nd isotopic data. Stratigraphy and Geological Correlation 7, 1–14.
Kovach, V.P., Kotov, A.B., Smelov, A.P., Staroseltsev, K.V., Salnikova, E.B., Zagornaya, N.Yu., Safronov, A.F., Pavlushin, A.D., 2000. Evolutionary stages of the continental crust in the buried basement of the eastern Siberian Platform: Sm–Nd isotopic data. Petrology 8, 353–365.
Kovach, V.P., Matukov, D.I., Berezhnaya, N.G., Kotov, A.B., Levitsky, V.I., Barash, I.G., Kozakov, I.K., Levsky, L.K., Sergeev, S.A., 2004. SHRIMP zircon age of the Gargan block tonalites – find early Precambrian basement of the Tuvino–Mongolian microcontinent, Central Asia Mobile Belt. 32th Intern. Geological Congress, Abstract.
Kovach, V.P., Jian, P., Yarmolyuk, V.V., Kozakov, I.K., Liu, D., Terent'eva, L.B., Lebedev, V.I., Kovalenko, V.I., 2005. Magmatism and geodynamics of early stages of the Paleo-Asian ocean formation: geochronological and geochemical data on ophiolites of the Bayan-Khongor zone. Doklady Earth Sciences 404, 1072–1077.
Kovach, V.P., Yarmolyuk, V.V., Kovalenko, V.I., Kozlovskii, A.M., Kotov, A.B., Terent'eva, L.B., 2011. Composition, sources, and growth mechanisms of continental crust in the Lake zone of the Central Asian Caledonides: II. Geochemical and Nd isotopic data. Petrology 19, 417–444.
Kovalenko, V.I., Yarmolyuk, V.V., Kovach, V.P., Kotov, A.B., Kozakov, I.K., Salnikova, E.B., 1996. Sources of Phanerozoic granitoids in central Asia: Sm–Nd isotope data. Geochemistry International 34, 628–640.
Kovalenko, V.I., Yarmolyuk, V.V., Kovach, V.P., Kotov, A.B., Kozakov, I.K., Salnikova, E.B., Larin, A.M., 2004. Isotope provinces, mechanism of generation and sources of the continental crust in the Central Asian Mobile Belt: geological and isotopic evidence. Journal of Asian Earth Sciences 23, 605–627.
Kozakov, I.K., Kotov, A.B., Kovach, V.P., Salnikova, E.B., 1997. Crustal growth in the geologic evolution of the Baidarik block, Central Mongolia: evidence from Sm–Nd isotopic systematics. Petrology 5, 201–207.
Kozakov, I.K., Kotov, A.B., Salnikova, E.B., Bibikova, E.V., Kovach, V.P., Kirnozova, T.I., Berezhnaya, N.G., Lykhin, D.A., 1999. Metamorphic age of crystalline complexes of the Tuva–Mongolia Massif: the U–Pb geochronology of granitoids. Petrology 7, 177–191.
Kozakov, I.K., Kotov, A.B., Salnikova, E.B., Kovach, V.P., Nutman, A., Bibikova, E.V., Kirnozova, T.I., Todt, W., Kroener, A., Yakovleva, S.Z., Lebedev, V.I., Sugorakova, A.M., 2001. Timing of the structural evolution of metamorphic rocks in the Tuva–Mongolian Massif. Geotectonics 35, 165–184.
Kozakov, I.K., Salnikova, E.B., Khain, E.V., Kovach, V.P., Berezhnaya, N.G., Yakovleva, S.Z., Plotkina, Yu.V., 2002. Early Caledonian crystalline rocks of the lake zone in Mongolia: formation history and tectonic settings as deduced from U-Pb and Sm-Nd datings. Geotectonics 36, 156–166.
Kozakov, I.K., Salnikova, E.B., Didenko, A.N., Kovach, V.P., Fedoseenko, A.M., Yakovleva, S.Z., 2004. The age and geodynamic setting of formation of high-temperature metamorphic complexes in the South Mongolian Belt. Russian Geology and Geophysics 45, 519–524.
Kozakov, I.K., Salnikova, E.B., Natman, A., Kovach, V.P., Kotov, A.B., Podkovyrov, V.N., Plotkina, Yu.V., 2005. Metasedimentary complexes of the Tuva–Mongolian Massif: age, provenances, and tectonic position. Stratigraphy and Geolological Correlation 13, 1–20.
Kozakov, I.K., Kovach, V.P., Bibikova, E.V., Kirnozova, T.I., Zagornaya, N.Yu., Plotkina, Yu.V., Podkovyrov, V.N., 2007a. Age and sources of granitoids in the junction zone of the caledonides and hercynides in Southwestern Mongolia: geodynamic implications. Petrology 15, 126–150.
Kozakov, I.K., Kovach, V.P., Salnikova, E.B., Kotov, A.B., 2007b. Geochronoly and Crustal Evolution of the Crystalline Complexes of the Central Asia. In: International Symposium on the Precambrian Chronology and Tectonic Evolution, Beijing, p. 14.
Kozakov, I.K., Sal'nikova, E.B., Wang, T., Didenko, A.N., Plotkina, Y.V., Podkovyrov, V.N., 2007c. Early Precambrian crystalline complexes of the central Asian microcontinent: age, sources, tectonic position. Stratigraphy and Geological Correlation 15, 121–140.
Kozakov, I.K., Salnikova, E.B., Kovach, V.P., Yarmolyuk, V.V., Anisimova, I.V., Kozlovskii, A.M., Plotkina, Yu.V., Myskova, T.A., Fedoseenko, A.M., Yakovleva, S.Z., Sugorakova, A.M., 2008. Vendian stage in formation of the early Caledonian superterrane in Central Asia. Stratigraphy and Geological Correlation 16, 360–382.
Kozakov, I.K., Kirnozova, T.I., Kovach, V.P., Plotkina, Yu.V., Fugzan, M.M., 2009a. Crystalline complexes of the Tarbagatai block of the Early Caledonian superterrane of the Central Asia: geodynamic consequences. In: IV Russian Conference on Isotope Geochronology, St-Petersburg, Conference Abstracts 1, pp. 246–249 (in Russian).
Kozakov, I.K., Anisimova, I.V., Salnikova, E.B., Kovach, V.P., 2009b. Ryphean metamorphic complex of the Songino block of the Early Caledonian superterrane of the Central Asia. In: IV Russian Conference on Isotope Geochronology, St-Petersburg, Conference Abstracts 1, pp. 249–251 (in Russian).
Kravchinsky, V.A., Sklyarov, E.V., Gladkochub, D.P., Harbert, W.P., 2010. Paleomagnetism of the Precambrian Eastern Sayan rocks: implications for the Ediacaran–Early Cambrian paleogeography of the Tuva–Mongolian composite microcontinent. Tectonophysics 486, 65–80.
Kröner, A., Windley, B.F., Badarch, G., Tomurtogoo, O., Hegner, E., Jahn, B.M., Gruschka, S., Khain, E.V., Demoux, A., Winjgate, M.T.D., 2007. Accretionary growth and crust-formation in the Central Asian Orogenic Belt and comparison with the Arabian–Nubian shield. Geological Society of America, Memoir 200, 181–209.
Kuzmichev, A.B., 2004. Tectonic History of the Tuva–Mongolian Massif: Early and Late Baikalian and Early Caledonian Stages. PROBEL Publishers, Moscow (in Russian).

Kuzmichev, A., Kröner, A., Hegner, E., Dunyi, L., Yusheng, W., 2005. The Shishkhid ophiolite, northern Mongolia: a key to the reconstruction of a Neoproterozoic island-arc system in central Asia. Precambrian Research 138, 125–150.

Kuzmichev, A., Sklyarov, E., Postnikov, A., Bibikova, E., 2007. The Oka Belt (Southern Siberia and Northern Mongolia): a Neoproterozoic analog of the Japanese Shimanto Belt? The Island Arc 16, 224–242.

Kuzmichev, A.B., Larionov, A.N., 2011. The Sarkhoi Group in East Sayan: Neoproterozoic (~770– 800 Ma) volcanic belt of the Andean type. Russian Geology and Geophysics 52, 685–700.

Levashova, N.M., Kalugin, V.M., Gibsher, A.S., Yff, J., Ryabinin, A.B., Meert, J.G., Malone, S.J., 2010. The origin of the Baydaric microcontinent, Mongolia: constraints from paleomagnetism and geochronology. Tectonophysics 485, 306–320.

Li, X.H., Li, W.X., Li, Z.X., Wang, J., 2005. Formation of the South China Block: evidence from Sibaoan orogenic magmatism. In: Wingate, M.T.D., Pisarevsky, S.A. (Eds.), Supercontinent and Earth Evolution Symposium. Geological Society Australia, Fremantle, p. 86 (abstract 81).

Li, Z.X. et al., 2008. Assembly, configuration, and break-up history of Rodinia: a synthersis. Precambrian Research 160, 179–210.

Ling, W., Gao, S., Zhang, B., Li, H., Liu, Y., Cheng, J., 2003. Neoproterozoic tectonic evolution of the northwestern Yangtze craton South China: implications for amalgamation and break-up of the Rodinia supercontinent. Precambrian Research 122, 111–140.

Long, X., Yuan, Ch., Sun, M., Kröner, A., Zhao, G., Wilde, S., Hu, A., 2011. Reworking of the Tarim Craton by underplating of mantle plume-derived magmas: evidence from Neoproterozoic granitoids in the Kuluketage area, NW China. Precambrian Research 187, 1–14.

Lu, S., Yuan, G., 2003. Geochronology of early Precambrian magmatic activities in Aketasdhtage, east Altyn Tagh. Journa Acta Geologyca Sinica 77, 61–68 (in Chinese).

Lu, S., Li, H., Zhang, C., Niu, G., 2008. Geological and geochronological evidence for the Precambrian evolution of the Tarim craton and surrounding continental fragments. Precambrian Research 160, 94–107.

Ludwig, K.R., 2003. Isoplot v.3.0: A Geochronological Toolkit for Microsoft Excel. Special Publication, No. 4. Berkeley Geochronology Center, 70pp.

Makrygina, V.A., Belichenko, V.G., Reznitskii, L.Z., 2007. Types of paleoisland arcs and back-arc basins in the northeast of the Paleoasian Ocean (from geochemical data). Russian Geology and Geophysics 48, 107–119.

Maruyama, S., Santosh, M., Zhao, D., 2007. Superplume, supercontinent and post-perovskite: mantle dynamics and anti-plate tectonics on the core–mantle boundary. Gondwana Research 11, 7–37.

Metcalfe, I., 2011. Tectonic framework and Phanerozoic evolution of Sundaland. Gondwana Research 19, 3–21.

Metelkin, D.V., Vernikovsky, V.A., Kazansky, A.Yu., 2007. Neoproterozoic evolution of Rodinia: constraints from new paleomagnetic data on the western margin of the Siberian. Russian Geology and Geophysics 48, 32–45.

Mossakovsky, A.A., Ruzhentsev, S.V., Samygin, S.G., Kheraskova, T.N., 1993. Central Asian Fold Belt: geodynamic evolution and formation history. Geotectonics 27, 445–473.

Münker, C., Weyer, S., Scherer, E., Mezger, K., 2001. Separation of high field strength elements (Nb, Ta, Zr, Hf) and Lu from rock samples for MC-ICPMS measurements. Geochemistry Geophysics Geosystems 2.

Neymark, L.A., Kovach, V.P., Nemchin, A.A., Morozova, I.M., Kotov, A.B., Vinogradov, D.P., Gorokhovsky, B.M., Ovchinnikova, G.V., Bogomolova, L.M., Smelov, A.P., 1993. Late Arhaean intrusive complexes in the Olekma granite–greenstone terrain (eastern Siberia): geochemical and isotopic study. Precambrian Research 62, 453–472.

Nokleberg, W.J., Badarch, G., Berzin, N.A., Diggles, M.F., Hwang, D.H., Khanchuk, A.I., Miller, R.J., Naumova, V.V., Obolenskiy, A.A., Ogasawara, M., Parfenov, L.M., Prokopiev, A.V., Rodionov, S.M., Yan, H., 2004. Digital Files for Northeast Asia Geodynamics, Mineral Deposit Location, and Metallogenic Belt Maps, Stratigraphic Columns, Descriptions of Map Units, and Descriptions of Metallogenic Belts. US Geological Survey Open-File Report, 2004-1252.

Nozhkin, A.D., Turkina, O.M., Bayanova, T.B., Berezhnaya, N.G., Larionov, A.N., Postnikov, A.A., Travin, A.V., Ernst, R.E., 2008. Neoproterozoic rift and within-plate magmatism in the Yenisei Ridge: implications for the breakup of Rodinia. Russian Geology and Geophysics 49, 503–519.

Nutman, A.P., Chernyshev, I.V., Baadsgaard, H., Smelov, A.P., 1992. The Aldan shield of Siberia, USSR: the age of its Archaean components and evidence for widespread reworking in the mid-Proterozoic. Precambrian Research 54, 195–210.

Panteeva, S.V., Gladkochoub, D.P., Donskaya, T.V., Markova, V.V., Sandimirova, G.P., 2003. Determination of 24 trace elements in felsic rocks by inductively coupled plasma mass spectrometry after lithium metaborate fusion. Spectrochimica Acta Part B: Atomic Spectroscopy 58, 341–350.

Parfenov, L.M., Khanchuk, A.I., Badarch, G., Miller, R.J., Naumova, V.V., Nokleberg, W.J, Ogasawara, M., Prokopiev, A.V., Yan, H., 2004. Northeast Asia Geodynamic Map, 2004. US Geological Survey Open-File Report 2004-1252.

Patchett, P.J., Kouvo, O., Hedge, C.E., Tatsumoto, M., 1981. Evolution of continental crust and mantle heterogeneity: evidence from Hf isotopes. Contribution to Mineralogy and Petrology 78, 279–297.

Petrova, Z.I., Reznitskii, L.Z., Makrygina, V.A., 2002. Geochemical parameters of metaterrigenous rocks of the Slyudyanka group, southwestern Baikal Area, as indicators of their source and protolith genesis. Geochemistry International 4, 355–365.

Petrova, Z.I., Makrygina, V.A., Reznitskii, L.Z., 2005. Geochemistry of metagraywackes in the structures surrounding the southern part of the Siberian Platform and their significance for paleogeodynamic reconstructions. Geochemistry International 8, 758–768.

Pfander, J.A., Jochum, K.P., Kozakov, I., Alfred Kröner, A., Todt, W., 2002. Coupled evolution of back-arc and island arc-like mafic crust in the late_Neoproterozoic Agardagh–Tes-Chem ophiolite, Central Asia: Evidence from trace element and Sr–Nd–Pb isotope data. Contribution to Mineralogy and Petrology 143, 154–174.

Pisarevsky, S.A., Natapov, L.M., Donskaya, T.V., Gladkochub, D.P., Vernikovsky, V.A., 2008. Proterozoic Siberia: a promontory of Rodinia. Precambrian Research 160, 66–76.

Poller, U., Gladkochub, D., Donskaya, T., Mazukabzov, A., Sklyarov, E., Todt, W., 2005. Multistage magmatic and metamorphic evolution in the Southern Siberian craton: Archean and Palaeoproterozoic zircon ages revealed by SHRIMP and TIMS. Precambrian Research 136, 353–368.

Qiu, Y.M., Gao, S., McNaughton, N.J., Groves, D.I., Ling, W., 2000. First evidence of >3.2 Ga continental crust in the Yangtze craton of south China and its implications for Archean crustal evolution and Phanerozoic tectonics. Geology 28 (1), 11–14.

Reznitskii, L.Z., Sklyarov, E.V., Uschapovskaya, Z.F., 1988. Cr and V minerals in the Slyudyansky crystalline complex. In: Precambrian metamorphic complexes of the Eastern Siberia. Novosibirsk, Nauka, pp. 63–74 (in Russian).

Reznitskii, L.Z., Khalilov, V.A., Vasil'ev, E.P., Bulina, V.A., 1991. First results of U–Pb isotopic studies of accessory zircons from the Slyudyanskiy complex granulites (Southern Transbaikalia). Transactions (Doklady) of the USSR Academy of Scienes 320, 957–962.

Reznitskii, L.Z., Shkol'nik, S.I., Levitskii, V.I., 2004. Geochemistry of calc-silicate rocks of the Kharagolskaya suite (Southern Transbaikalia). Litology and Ore Deposites 3, 271–285.

Rojas-Agramonte, Y., Kröner, A., Demoux, A., Xia, X., Wang, W., Donskaya, T., Liu, D., Sun, M., 2011. Detrital and xenocrystic zircon ages from Neoproterozoic to Palaeozoic arc terranes of Mongolia: significance for the origin of crustal fragments in the Central Asian Orogenic Belt. Gondwana Research 19, 751–763.

Rosen, O.M., Turkina, O.M., 2007. The oldest rock assemblages of the Siberian craton. In: Earth's Oldest Rocks. In: Martin, J., Van Kranendonk, J., Smithies, R.H., Bennett, V.C. (Eds.), Developments in Precambrian Geology 15, pp. 793–838.

Rudenko, V.E., Lokhov, I.K., Saltykova, T.E., Stepanov, D.V., Berezhnaya, N.G., 2007. Question about stability of U–Pb, Rb-Sr и Sm–Nd systems during polymetamorphic and tectono-magmatic transformations. Granulite complexes in geological development of Precambrian and Phanerozoic. In: II Russian Conference on Problems of Precambrian Geology and Geodynamic, St-Petersburg, pp. 274–275 (in Russian).

Rytsk, E.Yu., Amelin, Yu.V., Rizvanova, N.G., Krymsky, R.Sh., Mitrofanov, G.L., Mitrofanova, N.N., Perelyaev, V.I., Shalaev, V.S., 2001. Age of rocks of the Baikal-Muya fold belt. Stratigraphy and Geologucal Correlation 9, 3–15.

Rytsk, E.Yu., Shalaev, V.S., Rizvanova, N.G., Krymsky, R.Sh., Makeev, A.F., Rile, G.V., 2002. The Olokit zone of the Baikal Fold region: new isotopic geochronological and geochemical data. Geotectonics 36, 29–41.

Rytsk, E.Yu., Kovach, V.P., Yarmolyuk, V.V., Kovalenko, V.I., 2007. Structure and evolution of the continental crust in the Baikal fold region. Geotectonics 41, 440–464.

Rytsk, E.Yu., Kovach, V.P., Makeev, A.F., Bogomolov, E.S., Rizvanova, N.G., 2009. The eastern boundary of the Baikal collisional belt: geological, geochronological, and Nd isotopic evidence. Geotectonics 43, 264–273.

Safonova, I.Yu., Simonov, V.A., Buslov, M.M., Ota, T., Maruyama, Sh., 2008. Neoproterozoic basalts of the Paleo-Asian Ocean (Kurai accretion zone, Gorny Altai, Russia): geochemistry, petrogenesis, geodynamics. Russian Geology and Geophysics 49, 254–271.

Salnikova, E.B., Kovach, V.P., Kotov, A.B., Nemchin, A.A., 1996. Evolution of continental crust in the Western Aldan Shield: evidence from Sm–Nd systematics of granitoids. Petrology 2, 105–118.

Salnikova, E.B., Sergeev, S.A., Kotov, A.B., Yakovleva, S.Z., Steiger, R.H., Reznitskiy, L.Z., Vasil'ev, E.P., 1998. U–Pb zircon dating of granulite metamorphism in the Slyudyaskiy complex, Eastern Siberia. Gondwana Research 1, 195–205.

Salnikova, E.B., Kozakov, I.K., Kotov, A.B., Kroener, A., Todt, W., Bibikova, E.V., Nutman, A., Yakovleva, S.Z., Kovach, V.P., 2001. Age of Palaeozoic granites and metamorphism in the Tuvino–Mongolian Massif of the Central Asian Mobile Belt: loss of Precambrian microcontinent. Precambrian Research 110, 143–164.

Salnikova, E.B., Kotov, A.B., Levitsky, V.I., Reznitskii, L.Z., Melnikov, A.I., Kozakov, I.K., Kovach, V.P., Barash, I.G., Yakovleva, S.Z., 2007. Age constraints of high-temperature metamorphic events in crystalline complexes of the Irkut Block, the Sharyzhalgay ledge of the Siberian Platform basement: results of the U–Pb single zircon dating. Stratigraphy and Geological Correlation 15, 343–358.

Scherer, U., Corfu, F., Demaiffe, D., 1997. U–Pb and Lu–Hf isotopes in baddeleyite and zircon megacrysts from the Mbuji-Mayi kimberlite: constraints on the subcontinental mantle. Chemical Geology 143, 1–16.

Scherer, E.E., Cameron, K.L., Blichert-Toft, J., 2000. Lu–Hf garnet geochronology: closure temperature relative to the Sm–Nd system and the effects of trace mineral inclusions. Geochimica et Cosmochimica Acta 64, 3413–3432.

Scherer, E.E., Münker, C., Mezger, K., 2001. Calibration of the Lutetium–Hafnium Clock. Science 293, 683–687.

Sengör, A.M.C., Natal'in, B.A., Burtmann, V.S., 1993. Evolution of the Altaid tectonic collage and Palaeozoic crustal growth in Eurasia. Nature 364, 299–306.

Shafeev, A.A., 1970. Precambrian of the South-Western Transbaikalia and Khamar-Daban. Nauka, Moscow, 180pp. (in Russian).

Shaw, D.M., 1970. Trace element fractionation during anatexis. Geochimica et Cosmochimica Acta 34, 237–243.

Shu, L.S., Deng, X.L., Zhu, W.B., Ma, D.S., Xiao, W.J., in press. Precambrian tectonic evolution of the Tarim Block, NW China: new geochronological insights from the Quruqtagh domain. Journal of Asian Earth Sciences, doi:10.1016/j.jseaes.2010.08.018.

Stepanov, D.V., Lokhov, K.I., Rudenko, E.V., 2009. Isotope-geochemical basis of the age of carbonate rocks of the Slyudyansky crystalline complex. Isotope systems and time of geological processes. In: IV Russian Conference on Isotope Geochronology, Saint-Petersburg, Conference Abstracts 2, pp. 196–200 (in Russian).

Taylor, S.R., McLennan, S.M., 1985. The Continental Crust: Its Evolution and Composition. Blackwell, London, 312pp..

Tectonic Map of Northern Eurasia, 1979. Scale 1:5000000. GUGK, Moscow (in Russian).

Terent'eva, L.B., Kovach, V.P., Yarmolyuk, V.V., Kovalenko, V.I., Kozlovsky, A.M., 2008. Composition, sources, and geodynamis of rock formation in the late Riphean Bayankhongor ophiolite zone: characteristics of early stages in the evolution of the Paleo-Asian ocean. Doklady Earth Science 423A, 1462–1466.

Turkina, O.M., Noshkin, A.D., Bayanova, T.B., Dmitrieva, N.V., Travin, A.V., 2007. Precambrian terranes in the southwestern framing of the Siberian craton: isotopic provinces, stages of crustal evolution and accretion–collision events. Russian Geology and Geophysics 48, 61–70.

Turkina, O.M., Berezhnaya, N.G., Larionov, A.N., Lepekhina, E.N., Presnyakov, S.L., Saltykova, T.E., 2009. Paleoarchean tonalite–trondhjemite complex in the northwestern part of the Sharyzhalgay Uplift (southwestern Siberian craton): results of U–Pb and Sm–Nd study. Russian Geology Geophysics 50, 15–28.

Turkina, O.M., Urmantseva, L.N., Berezhnaya, N.G., Presnyakov, S.L., 2010. Paleoproterozoic age of the protoliths of metaterrigenous rocks in the east of the Irkut granulite–gneiss block (Sharyzhalgay salient, Siberian craton). Stratigraphy and Geological Correlation 18, 16–30.

Utsunomiya, A., Jahn, B.-M., Ota, T., Safonova, I.Yu., 2009. A geochemical and Sr–Nd isotopic study of the Vendian greenstones from Gorny Altai, southern Siberia: implications for the tectonic setting of the formation of greenstones and the role of oceanic plateaus in accretionary orogen. Lithos 113, 437–453.

Vasil'ev, E.P., Reznitskiy, L.Z., 1993. Early Precambrian complexes of the Khamar-Daban range. In: Kozakov, I.K. (Ed.), Early Precambrian of the Central Asian Fold Belt. Nauka, St-Petersburg, pp. 147–160 (in Russian).

Vasil'ev, E.P., Reznitskiy, L.Z., Vishnyakov, V.N., Nekrasova, E.A., 1981. Slyudyanskiy Crystalline Complex. Nauka, Novosibirsk, pp. 198 (in Russian).

Vernikovsky, V.A., Vernikovskaya, A.E., Kotov, A.B., Sal'nikova, E.B., Kovach, V.P., 2003. Neoproterozoic accretionary and collisional events on the western margin of the Siberian craton: new geological and geochronological evidence from the Yenisey Ridge. Tectonophysics 375, 147–168.

Vervoort, J.D., Patchett, P.J., 1996. Behavior of hafnium and neodymium isotopes in the crust: constraints from Precambrian crustally derived granites. Geochimica et Cosmochimica Acta 60, 3717–3733.

Volobuev, M.I., Zykov, S.I., Stupnikova, N.I., 1980. Geochronology of the Precambrian granitoids of the Eastern Sayan and Western Transbaikalia. In: Geochronology of the Eastern Siberia and Far East. Nauka, Moscow, pp. 66–79.

Wan, Y., Liu, D., Wang, S., Dong, C., Yang, E., Wang, W., Zhou, H., Ning, Z., Du, L., Yin, X., Xie, H., Ma, M., 2010. Juvenile magmatism and crustal recycling at the end of Neoarchean in Western Shandong Province, North China craton: evidence from SHRIMP zircon dating. American Journal of Science 310, 1503–1552.

Wang, T., Zheng, Ya., Gehrels, G.E., Mu, Z., 2001. Geochronological evidence for existence of South Mongolian microcontinent – a zircon U-Pb age of granitoid gneisses from the Yagan-Onch Hayrhan metamorphic core complex. China Science Bulletine 146, 2005–2008.

Wiedenbeck, M.P.A., Corfu, F., Griffin, W.L., Meier, M., Oberli, F., von Quadt, A., Roddick, J.C., Spiegel, W., 1995. Three natural zircon standards for U–Th–Pb, Lu–Hf, trace element and REE analyses. Geostandards and Geoanalytical Research 19, 1–23.

Windley, B.F., Alexeiev, D., Xiao, W.J., Kröner, A., Badarch, G., 2007. Tectonic models for accretion of the Central Asian Orogenic Belt. Journal of the Geological Society of London 164, 31–47.

Woodhead, J.D., Hergt, J.M., 2005. A preliminary appraisal of seven natural zircon reference materials for in situ Hf isotope determination. Geostandards and Geoanalytical Research 29, 183–195.

Wu, F., Zhao, G., Wilde, S.A., Simon, A., Sun, D., 2005. Nd isotopic constraints on crustal formation in the North China craton. Journal of Asian Earth Sciences 24, 523–545.

Yarmolyuk, V.V., Kovalenko, V.I., 2001. Late Riphean breakup between Siberia and Laurentia: evidence from intraplate magmatism. Doklady Earth Science 379, 526–528.

Yarmolyuk, V.V., Kovalenco, V.I., Salnikova, E.B., Kozakov, I.K., Kotov, A.B., Kovach, V.P., Vladykin, N.V., Yakovleva, S.Z., 2005a. U–Pb age of syn- and post-metamorphic granitoids of south Mongolia: evidence for the presence of Grenvillides in the Central Asian Fold Belt. Doklady Earth Sciences 404, 986–990.

Yarmolyuk, V.V., Kovalenko, V.I., Sal'nikova, E.B., Nikiforov, A.V., Kotov, A.B., Vladykin, N.V., 2005b. Late Riphean rifting and breakup of Laurasia: data on geochronological studies of ultramafic alkaline complexes in the Southern framing of the Siberian craton. Doklady Earth Sciences 404, 1031–1036.

Yarmolyuk, V.V., Kovalenko, V.I., Kovach, V.P., Rytsk, E.Yu., Kozakov, I.K., Kotov, A.B., Salnikova, E.B., 2006. Early stages of the Paleoasian ocean formation: results of geochronological, isotopic, and geochemical investigations of late Riphean and Vendian–Cambrian complexes in the Central Asian Foldbelt. Doklady Earth Sciences 411, 1184–1189.

Yarmolyuk, V.V., Kovalenko, V.I., Anisimova, I.V., Sal'nikova, E.B., Kovach, V.P., Kozakov, I.K., Kozlovsky, A.M., Kudryashova, E.A., Kotov, A.B., Plotkina, Y.V., Terent'eva, L.B., Yakovleva, S.Z., 2008. Late Riphean alkali granites of the Zabhan microcontinent: evidence for the timing of Rodinia breakup and formation of microcontinents in the Central Asian Fold Belt. Doklady Earth Sciences 420, 583–588.

Yarmolyuk, V.V., Kozakov, I.K., Anisimova, I.V., Sal'nikova, E.B., Kovach, V.P., Kozlovsky, A.M., Plotkina, Y.V., Terent'eva, L.B., Yakovleva, S.Z., 2009. Valuation of age of the ophiolite complex in the Songino uplift of the Early Caledonian superterrane of the Central Asia. In: IV Russian Conference on Isotope Geochronology. St.-Petersburg, Conference Abstracts 2, pp. 294–296 (in Russian).

Yarmolyuk, V.V., Kovach, V.P., Kovalenko, V.I., Salnikova, E.B., Kozlovskii, A.M., Kotov, A.B., Yakovleva, S.Z., Fedoseenko, A.M., 2011. Composition, sources, and growth mechanisms of continental crust in the Lake zone of the Central Asian Caledonides: I. Geological and geochronological data. Petrology 19, 55–78.

Zhai, M., Guo, J., Liu, W., 2005. Neoarchean to Paleoproterozoic continental evolution and tectonic history of the North China craton: a review. Journal of Asian Earth Sciences 24, 547–561.

Zhang, S.B., Zheng, Y.F., Wu, Y.B., Zhao, Z.F., Gao, S., Wu, F.Y., 2006. Zircon isotope evidence for >3.5 Ga continental crust in the Yangtze craton of China. Precambrian Research 146, 16–34.

Zhao, G.C., Sun, M., Wilde, S.A., Li, S.Z., 2005. Late Archean to Paleoproterozoic evolution of the North China craton: key issues revisited. Precambrian Research 136, 177–202.

Zonenshain, L.P., Kuzmin, M.I., Natapov, L.M., 1990. Geology of the USSR: a plate-tectonic synthesis. In: Geodynamics Series, vol. 21. American Geophysical Union, Washington, DC, 242 pp.